JOURNAL OF COMPUTATIONAL PHYSICS 79, 12–49 (1988)

Fronts Propagating with Curvature-Dependent Speed: Algorithms Based on Hamilton–Jacobi Formulations

STANLEY OSHER*

Department of Mathematics, University of California, Los Angeles, California 90024

AND

JAMES A. SETHIAN†

Department of Mathematics, University of California, Berkeley, California 94720

Received June 3, 1987; revised November 11, 1987

We devise new numerical algorithms, called PSC algorithms, for following fronts propagating with curvature-dependent speed. The speed may be an arbitrary function of curvature, and the front also can be passively advected by an underlying flow. These algorithms approximate the equations of motion, which resemble Hamilton–Jacobi equations with parabolic right-hand sides, by using techniques from hyperbolic conservation laws. Nonoscillatory schemes of various orders of accuracy are used to solve the equations, providing methods that accurately capture the formation of sharp gradients and cusps in the moving fronts. The algorithms handle topological merging and breaking naturally, work in any number of space dimensions, and do not require that the moving surface be written as a function. The methods can be also used for more general Hamilton–Jacobi-type problems. We demonstrate our algorithms by computing the solution to a variety of surface motion problems.

1. INTRODUCTION

In a variety of physical phenomena, one wants to track the motion of a front whose speed depends on the local curvature. Two well-known examples are crystal growth [3, 19, 20, 24, 25, 30, 38] and flame propagation [6, 18, 22, 23, 37, 40]. In this paper, we introduce, analyze, and utilize a collection of new numerical algorithms for studying such problems. These new algorithms approximate the

* Supported by NSF Grant DMS85-03294, DARPA Grant in the ACMP Program, ONR Grant N00014-86-K-0691.

† Supported by the Applied Mathematics Subprogram of the Office of Energy Research under contract DE-AC03-76SF00098, the National Science Foundation, and the Sloan Foundation.

0021-9991/88 $3.00

equations of motion of propagating fronts, which resemble Hamilton–Jacobi equations with viscosity terms. We demonstrate our algorithms by computing the solutions to a variety of surface motion problems.

The background theory and numerical experimentation behind this approach have been developed in a series of papers, see [31–34]. In this paper, these ideas are coupled to the technology for the numerical approximation of hyperbolic conservation laws to produce algorithms which we call PSC schemes, for propagation of surfaces under curvature. These new schemes allow one to follow the motion of an N–1 dimensional surface in N space dimensions. The speed may be an arbitrary function of the curvature, and the front also can be passively advected by an underlying flow. The algorithms can be constructed with any desired accuracy in space and time and do not require the front to remain a function. The methods are set in an Eulerian framework; thus the number of computational elements is fixed at the outset. Topological merging and breaking is handled naturally, and the basic first-order scheme is extremely simple to program.

As illustration of the wide applicability of such algorithms, consider the case of flame propagation, see [34]. A common model idealizes the burning flame as an infinitely thin boundary which separates regions of constant steady-state velocity, density, and temperature, and propagates into the unburnt fluid at a speed dependent on the local curvature. The idea here is that cool convex fingers reaching out into the unburnt gas somehow propagate slower than do concave regions which are hot gases surrounding a small unburnt pocket. At the same time, particles along the flame front undergo an increase in volume as they burn, creating a jump in velocity across the flame front. This discontinuity in the velocity field creates vorticity along the burning flame, which can be related to the local curvature, and this new vorticity field contributes to the advection of the propagating flame. Thus, there are at least two distinct ways in which the speed of the moving flame depends on the local curvature.

Typically, there have been two types of numerical algorithms employed in the solution of such problems. The first parametrizes the moving front by some variable and discretizes this parametrization into a set of marker points [39]. The positions of the marker points are updated in time according to approximations to the equations of motion. Such techniques can be extremely accurate in the attempt to follow the motions of small perturbations. However, for large, complex motion, several problems soon occur. First, marker particles come together in regions where the curvature of the propagating front builds, causing numerical instability unless a regridding technique is employed. The regridding mechanism usually contains an error term which resembles diffusion and dominates the real effects of curvature under analysis. Second, such methods suffer from topological problems; when two regions "burn" together to form a single one, ad hoc techniques to eliminate parts of the boundary are required to make the algorithm work.

Other algorithms commonly employed fall under the category of "volume of fluid" techniques, which, rather than track the boundary of the propagating front, track the motion of the interior region. An example of this type of algorithm is

SLIC [26]. In these algorithms, the interior is discretized, usually by employing a grid on the domain and assigning to each cell a "volume fraction" corresponding to the amount of interior fluid currently located in that cell. An advantage of such techniques is that no new computational elements are required as the calculation progresses (unlike the parametrization methods), and complicated topological boundaries are easily handled, see [4, 32]. Unfortunately, it is difficult to calculate the curvature of the front from such a representation of the boundary.

The central idea in this paper is the formulation of the correct equation of motion for a front propagating with curvature-dependent speed. This equation is an initial-value Hamilton–Jacobi equation with right-hand side that depends on curvature effects. The limit of the right-hand side as the curvature effects go to zero is an eikonal equation with an associated entropy condition. By viewing the surface as a level set, topological complexities and changes in the moving front are handled naturally. With these equations as a basis, any number of numerical algorithms may be devised for an arbitrary degree of accuracy, using the technology developed for the solution of hyperbolic conservation laws. In particular, algorithms can be devised to have the correct limiting entropy-satisfying solution. In fact, some previous algorithms may be viewed as less sophisticated approximations to our equations of motion.

The evolution of this approach is somewhat interesting. Motivated by the use of SLIC [26] in a Huyghen's principle flame propagation scheme [4], in [31] an entropy condition was formulated for moving fronts. In [31], it was then shown that the Huyghen's approach was an approximation to the eikonal equation, which is a constant coefficient Hamilton–Jacobi equation with zero right-hand side, and that the postulated entropy condition occurs naturally in this equation. Viewed from the eikonal framework, the inherent instability of marker particles was shown and demonstrated, see [31, 34]. We then studied the effects of curvature on a propagating front and showed in [32, 33, 35] that curvature added a parabolic right-hand side to the Hamilton–Jacobi equations of motion. Numerical evidence was given in [32] showing that the entropy condition formulated in [31] picked out the correct viscous limit as the curvature effects vanished. Attempts to approximate the solution to these equations using Lax–Friedrichs were satisfactory; however, the use of centered differences created spurious boundary conditions. This then led naturally to the higher dimensional formulation and introduction of the higher order upwind schemes employed here.

The outline of this paper is as follows. In Section II, we give the equations of motion for propagating curves and surfaces in a form appropriate for numerical discretization. We then describe some past work, provide new proofs of some previous results, and present some new work. In Section III, we give background for the numerical methods for hyperbolic conservation schemes to be used and show how they can be used to provide solutions to Hamilton–Jacobi equations. In Sections IV and V, we use these techniques to approximate solutions to a variety of problems involving propagating curves and surfaces. In Appendix A, we discuss the inherent difficulty (linear ill-posedness) that any marker particle discretization (without

regridding) must encounter. In Appendix B, we construct the essential non-oscillatory interpolant used in high-order accurate approximation for general Hamilton–Jacobi equations.

II. Preliminary Analysis

We present the equations of motion and some theoretical results about curves and surfaces moving with curvature-dependent speed. We follow the analysis in [32] and begin with a simple, smooth, closed initial curve $\gamma(0)$ in R^2. Let $\gamma(t)$ be the one-parameter family of curves, where $t \in [0, \infty)$ is time, generated by moving the initial curve along the normal vector field with speed F, where F is a function of the curvature K. Let $X(s, t) = (x(s, t), y(s, t))$ be the position vector which parametrizes $\gamma(t)$ by s, $0 \leqslant s \leqslant S$, $X(0, t) = X(S, t)$. The curve is parametrized so that the interior is on the left in the direction of increasing s. With $K(s, t)$ as the curvature at $X(s, t)$, the equations of motion can be written as

$$x_t = F(K)\frac{y_s}{(x_s^2 + y_s^2)^{1/2}}, \qquad y_t = -F(K)\frac{x_s}{(x_s^2 + y_s^2)^{1/2}}, \tag{2.1}$$

to be solved for $t \in [0, \infty)$ with $X(s, 0) = \gamma(0)$, $s \in [0, S]$ given. Here, the curvature K is defined to be $K = (y_{ss}x_s - x_{ss}y_s)/(x_s^2 + y_s^2)^{3/2}$. Given the mapping from $[0, S]x[0, \infty)$ to R^2 generated by the moving curve, there exists near $t = 0$ an inverse mapping function f defined by $t = f(x, y)$. The curvature K can be written in terms of this function f as

$$K = \left(\frac{f_{xx}f_y^2 - 2f_{xy}f_xf_y + f_{yy}f_x^2}{(f_x^2 + f_y^2)^{3/2}}\right).$$

Our first result is

Proposition 2.1. *f satisfies the partial differential equation*

$$F^2(f_x^2 + f_y^2) = 1 \tag{2.2}$$

as long as the curve γ stays smooth and non-intersecting.

Proof. The Jacobian of the mapping defined through Eq. (2.1) is

$$J = \begin{bmatrix} x_t & y_t \\ x_s & y_s \end{bmatrix} = F(K)(x_s^2 + y_s^2)^{1/2},$$

where K is the curvature in Cartesian coordinates. As long as this map stays smooth and one to one, we have $f_x^2 + f_y^2 = t_x^2 + t_y^2 = y_s^2/J^2 + x_s^2/J^2 = 1/F^2$, which completes the proof.

We notice that Eq. (2.2) is, in general, a *second-order* nonlinear partial differential equation to be solved in (x, y, f) space near $(x_0(s), y_0(s), 0)$, yet we are only given initial data $f(x_0(s), y_0(s)) = \text{constant}$ on the initial curve and no information about the normal derivative of f on this curve. This seemingly paradoxical situation is resolved by

PROPOSITION 2.2. *Given a constant t_0, let γ_0 be the level curve of f, i.e.,*

$$t_0 = f(x_0(s), y_0(s)).$$

Then γ_0 is a characteristic curve for Eq. (2.2).

Proof. Differentiating f along γ with respect to s gives $f_x x_s + f_y y_s = 0$. Differentiating with respect to s again yields $f_{xx}(x_s^2) + 2f_{xy} x_s y_s + f_{yy}(y_s^2) + f_x x_{ss} + f_y y_{ss} = 0$. Using the former, we may write $x_s = \alpha f_y$, $y_s = -\alpha f_x$ for some $\alpha(s) \neq 0$, which, using the latter, gives us

$$K = -\frac{(f_x x_{ss} + f_y y_{ss})}{\alpha^2 (f_x^2 + f_y^2)^{3/2}}.$$

Thus, the required second derivatives of f are uniquely determined on the curve from f_x and f_y, which in turn are obtained uniquely from the above. This completes the proof.

Following [32] we define the metric $g(s, t) = (x_s^2 + y_s^2)^{1/2}$ and the angle $\theta = \tan^{-1}(y_s/x_s)$. A simple calculation gives us $\theta_s = gK$. We differentiate Eq. (2.1) with respect to s and rewrite the resulting system, using g and θ, as

$$g_t = \theta_s F(\theta_s/g) \tag{2.3}$$

$$\theta_t = \frac{-1}{g} \frac{\partial}{\partial s} F\left(\frac{\theta_s}{g}\right). \tag{2.4}$$

Define the variation of the front at time t by

$$\text{Var}(t) = \int_0^S |K(s, t)|\, g(s, t)\, ds = \int_0^S |\theta_s|\, ds.$$

Using this formulation, we generalize a result that first appeared in [32].

PROPOSITION 2.3. *Consider a curve moving with speed $F(K)$ via Eq.* (2.1). *Assume $F'(0) \leqslant 0$ and θ remains in the class* $\text{BV}[[0, S] \times [0, T]]$ *for $0 \leqslant t \leqslant T$. Then $(d/dt)\,\text{Var}(t) \leqslant 0$.*

Proof. The idea of the proof for smooth functions goes back to Oleinik [28] and was generalized by Kruz'kov [17] to the present class of functions. We shall

mimic Oleinik's proof only—the more general BV case follows as in [17]. Let $H(s, t) = 1$ if $\theta_s(s, t) > 0$, -1 if $\theta_s(s, t) < 0$, and 0 if $\theta_s(s, t) = 0$. Then,

$$\frac{\partial}{\partial t}\int_0^S |\theta_s|\, ds = \frac{\partial}{\partial t}\int_0^S \theta_s H\, ds = \int_0^S \theta_{st} H\, ds$$
$$= \int_0^S \left(-\frac{\partial}{\partial t}\left(\frac{1}{g}\frac{\partial}{\partial s} F\left(\frac{\theta_s}{g}\right)\right)\right) H\, ds.$$

Let $[s_i, s_{i+1}]$ be an interval on which $\theta_s > 0$ with θ_s vanishing at the end points. Then

$$\int_{s_i}^{s_{i+1}} \left(-\frac{\partial}{\partial s}\frac{1}{g}\frac{\partial}{\partial_s} F\left(\frac{\theta_s}{g}\right)\right) H\, ds$$
$$= F'\left(\frac{\theta_s}{g}\right)\frac{g_s}{g^3}\theta_s \Big|_{s_i}^{s_{i+1}} - F'\left(\frac{\theta_s}{g}\right)\frac{\theta_{ss}}{g^2}\Big|_{s_i}^{s_{i+1}}.$$

The first term on the right vanishes because $\theta_s = 0$ at each end point; the second term is non-positive because $-F'(0) \geqslant 0$ and $\theta_{ss}(s_{i+1}) \leqslant 0 \leqslant \theta_{ss}(s_i)$. A similar argument works on intervals for which $\theta_s < 0$ in the interior and θ_s vanishes at the end points. This completes the proof.

Using Eqs. (2.3) and (2.4), we have

$$K_t = -\left[\frac{\partial}{\partial s} F(K)/g\right]_s \frac{1}{g} - K^2 F(K).$$

Letting $F = 1 - \varepsilon K$, we obtain, as in [32],

$$K_t = \varepsilon K_{ss} + \varepsilon K^3 - K^2, \tag{2.5}$$

and, for $\varepsilon = 0$,

$$K(s, t) = \frac{K(s, 0)}{(1 + tK(s, 0))}.$$

This becomes infinite in finite time if $K(s, 0)$ is anywhere negative and is analogous to shock formation experienced in the single scalar convex conservation law. More precisely, consider the "viscous" conservation law with G concave, namely

$$u_t + [G(u)]_x = \varepsilon u_{xx}. \tag{2.6}$$

If we take $\varepsilon = 0$ (the shock case), weak solutions to

$$\begin{aligned} u_t + [G(u)]_x &= 0 \\ u(x, 0) &= u_0(x) \end{aligned} \tag{2.7}$$

are not unique, and an additional entropy condition is needed to select the correct viscosity limit. In order to assure that the solution to Eq. (2.7) be the unique limit as $\varepsilon \to 0$ of Eq. (2.6), any of an equivalent class of entropy conditions is imposed [17, 21, 28]. The relevant one for our purposes is geometric, namely that characteristics flow *into* a shock in the direction of increasing time. This means, for a piecewise continuous weak solution $u(x, t)$ having a jump moving with

$$\frac{dx}{dt} = S(t) = \frac{G(u_l) - G(u_r)}{u_l - u_r},$$

that $G'(u_l) > S > G'(u_r)$.

For the moving curve problem Eq. (2.1), or equivalently, Eq. (2.2), with $F = 1$, we need an entropy condition which yields the unique limit solution as $\varepsilon \to 0$, of the problem with $F = 1 - \varepsilon K$. Imagine the curve γ as a flame separating a burnt region on the inside from an unburnt region on the outside, and an indicator function for the burnt region was defined to be $\phi(x, y, t) = 1$ if the particle at (x, y) is burnt at time t, and zero otherwise. In [31] the following entropy condition was suggested: if $\phi(x, y, t^*) = 1$, then $\phi(x, y, t) = 1$ for $t > t^*$; i.e., once a particle is burnt it remains burnt. This was shown to be equivalent to requiring that ignition curves flow into corners. In [32] numerical evidence was provided to show that the weak solution generated by this entropy condition is indeed the correct limiting solution. We now prove that this is so.

We consider a small section of the curve $t = f(x, y)$, which, without loss of generality, we can write as $y = Y(x, t)$. We insert this into the expression $f_x^2 + f_y^2 = 1/F^2$, arriving at

$$Y_t = (1 + Y_x^2)^{1/2} \left(1 + \frac{\varepsilon Y_{xx}}{(1 + Y_x^2)^{3/2}} \right). \tag{2.8}$$

Here, we have also chosen a positive square root. Letting $u = Y_x$ and taking the x derivative of the above, we have [33]

$$u_t + [G(u)]_x = \varepsilon \frac{\partial}{\partial x} \left[\frac{u_x}{G(u)^2} \right] \tag{2.9}$$

for $G(u) = -(1 + u^2)^{1/2}$, $G(u)$ concave. The criterion for the inviscid limit problem given in [31] is easily seen to be that characteristics propagate into *shocks* for Eq. (2.9) with $\varepsilon = 0$, that is, into *corners* for Eq. (2.8) with $F = 1$. For concave $G(u)$, this is well known to be equivalent to the statement that limits of solutions to Eq. (2.9) (and thus Eq. (2.8)) converge to solutions satisfying this criterion [21].

We may rewrite Eq. (2.8) in the following form, namely

$$Y_t - \left[1 + \frac{\varepsilon Y_{xx}}{(1 + Y_x^2)^{3/2}} \right] ([1 + Y_x^2]^{1/2}) = 0$$

which is a Hamilton–Jacobi equation with second-order viscosity. For the more general case of a speed function $F(K)$, we have

$$Y_t - F\left[\frac{-Y_{xx}}{(1+Y_x^2)^{3/2}}\right](1+Y_x^2)^{1/2} = 0 \tag{2.10}$$

which is also a Hamilton–Jacobi equation with second-order perturbation if the speed function F satisfies (1) $F(0) \neq 0$ and (2) $F'(0) \neq 0$.

This formulation can be used to devise a numerical algorithm to approximate the solution of a curve propagating with curvature-dependent speed, as long as the front remains a function, using the advanced technology for shock dynamics. However, there is a different formulation of the problem which yields a different Hamilton–Jacobi-type equation and does not require that the propagating front remain a function. Define a Lipschitz continuous function $\phi(x, y, t)$ so that at $t = 0$, $\phi(x, y, 0) > 1$ inside the burnt region Ω, i.e., the region bounded by $\gamma(0)$, $\phi(x, y, 0) < 1$ outside Ω, and $\phi(x, y, 0) = 1$ on $\partial\Omega$. Next, let $\phi(x, y, t)$ be defined by $\phi(x, y, t) \equiv C$, where $t = f(x, y)$ is defined from Eq. (2.2) for any fixed constant C. This yields

$$f_x = \frac{-\phi_x}{\phi_t}, \qquad f_y = \frac{-\phi_y}{\phi_t},$$

and hence $F^2(\phi_x^2 + \phi_y^2) = \phi_t^2$. Thus, choosing the direction of propagation to be outwards, we have

$$\phi_t - F(K)(\phi_x^2 + \phi_y^2)^{1/2} = 0, \tag{2.11}$$

where

$$F = F(K) = F\left(\frac{-(\phi_{xx}\phi_y^2 - 2\phi_{xy}\phi_x\phi_y + \phi_{yy}\phi_x^2)}{(\phi_x^2 + \phi_y^2)^{3/2}}\right).$$

This is also a Hamilton-Jacobi equation with second-order right-hand side. However, this different formulation allows us to compue the solution even when the front is not a function and when two "burnt" regions merge together.

Using this formulation, and the recent theory of viscosity solutions to Hamilton–Jacobi equations, Barles [1] has proven that the entropy condition in [31] picks out the unique viscosity solution even when the front is not a function. He defines $\phi(x, y, 0) = (1 - d(x, y; \Omega))^+ + d(x, y; \Omega^c)$, where $x^+ = \max(x, 0)$ and Ω^c is the complement of Ω, and evolves ϕ according to Eq. (2.11) in the special case $F = 1$. He then chooses the unique viscosity solution which is characterized by the entropy condition of Crandall–Lions [5] and shows that the resulting surface $\gamma(t) = \partial\Omega_t$, defined by $\partial\Omega_t = (x, y, |\phi(x, y, t) = 1)$, evolves according to the entropy condition in [31].

Our results easily extend to initial surfaces. Suppose the surface $\gamma(0) =$

$(x(s_1, s_2), y(s_1, s_2), z(s_1, s_2))$, moves along its normal vector field with speed $F(K)$, yielding $\gamma(s_1, s_2, t) = \gamma(t)$. It may be rewritten as $t = f(x, y, z)$, where $F^2(f_x^2 + f_y^2 + f_z^2) = 1$. Here, $F = F(K)$, where

$$K = \frac{1}{(f_x^2 + f_y^2 + f_z^2)^{3/2}} \det \begin{pmatrix} f_{xx} & f_{xy} & f_{xz} \\ f_{yx} & f_{yy} & f_{yz} \\ f_{zx} & f_{zy} & f_{zz} \end{pmatrix},$$

if we use the Gaussian curvature, and

$$K = \frac{(f_{xx}(f_y^2 + f_z^2) + f_{yy}(f_x^2 + f_z^2) + f_{zz}(f_x^2 + f_y^2) - 2f_{xy}f_xf_y - 2f_{xz}f_xf_z - 2f_{yz}f_yf_z)}{(f_x^2 + f_y^2 + f_z^2)^{3/2}},$$

if we choose the mean curvature. Following the previous discussion for the propagating curve, we may focus on a small section of the initial surface and produce an evolution equation of the form

$$Y_t - F(K)(1 + Y_x^2 + Y_y^2)^{1/2} = 0, \tag{2.12}$$

where $z = Y(x, y, t)$ and K is the chosen form of the curvature. At the same time, we may once again view the initial surface as a level set of the function $\phi(x, y, z, t) = C$. More generally, to move an n-dimensional surface $f(x, \ldots, x_n) = t$, we are led to the Hamilton–Jacobi-like problem

$$\phi_t - F(K)\,|\nabla\phi| = 0 \tag{2.13}$$

with initial data

$$\phi(\bar{x}, 0) = (1 - d(\bar{x}, \Omega))^+ + d(\bar{x}, \Omega),$$

where $\phi(x_1, \ldots, x_n, t) = 1$, and the curvature is chosen appropriately. Of course, it is crucial that our numerical scheme pick out, when necessary, the correct entropy condition.

III. Numerical Methods

We have seen that the problem of following a front moving with curvature-dependent speed becomes a Hamilton–Jacobi equation with second-order right-hand side. Given an $(n-1)$-dimensional surface propagating in R^n, we have two formulations, namely

(1) Eq. (2.12), which is a Hamilton–Jacobi-type equation for Y in $N = n - 1$ space variables and applies when the front can be written as a function or

(2) Eq. (2.13), which is a Hamilton–Jacobi-type equation for ϕ in $N = n$ space variables and applies regardless of whether the front can be written as a function.

Thus, PSC algorithms, or propagation of surfaces under curvature algorithms, rely on approximaton of

$$\psi_t + H(D\psi) = 0 \qquad (3.1)$$
$$\psi(x, 0) = \psi_0(x)$$

with $D\psi = \psi_{x_1}, ..., \psi_{x_n}$, where we have written the equations for the case $F(K) = 1$ for simplicity. In Formulation (1),

$$H(u_1, ..., u_N) = -(1 + u_1^2 + \cdots + u_N^2)^{1/2}, \qquad (3.2)$$

whereas in Formulation (2),

$$H(u_1, ..., u_N) = -(u_1^2 + \cdots + u_N^2)^{1/2}. \qquad (3.3)$$

While Formulation (2) is more general, formulation (1) requires one less dimension, and thus is less time-consuming from the point of view of numerical computations. In this section, we describe numerical methods that can be used to approximate the solution to Eq. (3.1). First, we describe first-order monotone methods for one dimension, followed by higher order models. Then we present algorithms for first-order monotone methods for several dimensions, followed by higher order schemes. We then show how these schemes can be used to solve the general case of speed function $F(K)$. Initialization and boundary conditions are then discussed, followed by the extension of the algorithm to propagation plus passive advection.

A. *One Space Dimension*

(1) *First-Order Schemes for One Space Dimension*

In one space dimension, the technology for single conservation laws goes over almost directly. We differentiate Eq. (3.1) with respect to the single space variable x and let $u = \psi_x$ to produce

$$u_t + [H(u)]_x = 0. \qquad (3.4)$$

An algorithm to approximate the solution to the above is said to be in *conservation form* (that is, conserves u) if it can be written in the form

$$u_j^{n+1} = u_j^n - \Delta t/\Delta x(g_{j+1/2}^n - g_{j-1/2}^n). \qquad (3.5)$$

Here, the numerical flux function $g_{j+1/2} = g(u_{j-p+1}, ..., u_{j+q+1})$ must be Lipschitz and satisfy the consistency requirement $g(u, ..., u) = H(u)$. From here on, let $\psi(\Psi)$ be the exact (approximate) solution to Eq. 3.1.

A scheme is called *monotone* if the right-hand side of Eq. (3.5) is a non-decreasing

function of all its arguments. It can be shown that conservative monotone schemes have no spurious overshoots nor wiggles near discontinuities [16] and obey an entropy condition for limit solutions. In view of the link between the Hamilton–Jacobi equation and the conservation law equation in one space variable, we may easily adapt first-order monotone schemes for shock equations to our problem. In fact, both the scheme design and the theory go over word-for-word. The easiest way to see this is as follows. Let

$$\Psi^n_{j+1/2} = \sum_{v=-\infty}^{j} u^n_v \, \Delta x$$

(assuming u^n_j is zero for large $|j|$). Then summing Eq. (3.5) from $-\infty$ to j gives us

$$\Psi^{n+1}_{j+1/2} = \Psi^n_{j+1/2} - \Delta t \; g(D_- \Psi^n_{j-p+3/2}, \ldots, D_+ \Psi^n_{j+q+1/2}).$$

Here, we are using the operators D_- and D_+ defined by

$$D_- u_j = u_j - u_{j-1}, \qquad D_+ u_j = u_{j+1} - u_j.$$

Next, we shift the index $j+1/2$ to j, arriving at

$$\Psi^{n+1}_j = \Psi^n_j - \Delta t \; g(D_- \Psi^n_{j-p+1}, \ldots, D_+ \Psi^n_{j+q}).$$

Thus, any conservation form approximation to Eq. (3.4) of the form given in Eq. (3.5), and any convergence theory for Eq. (3.4), (see, for example, [16]), goes over directly. Possible numerical fluxes g will be described below.

We emphasize that the above summation is a purely mental exercise used to construct approximations to Eq. (3.1) in one space dimension. Thus, the following discussion of conservation form approximations to Eq. (3.4) will lead us to appropriate approximations to Eq. (3.1) in more than one space dimension. The simplest scheme is Lax–Friedrichs, which relies on a central difference approximation to g, and preserves monotonicity through a second-order linear smoothing term. Unfortunately, this scheme is not upwind (to be described later), and this will turn out to be a critical requirement for boundaries.

Thus, we begin with the canonical upwind monotone scheme, namely Godunov's method [12]. A key aspect of this scheme is that the flux function g is the least viscous of all 2-point monotone fluxes [27]. In this scheme, g is constructed as follows. View the data $[u^n_j]_{j=-\infty}^{\infty}$ as representing a piecewise constant function:

$$u_\Delta(x; t_n) \equiv u^n_j, \qquad x_{j-1/2} \leqslant x \leqslant x_{j+1/2}. \tag{3.6}$$

For $\Delta t/\Delta x$ small enough, the initial value problem Eq. (3.4) with $u(x, 0) = u_\Delta(x; t_n)$ is a sequence of connected Riemann problems; i.e., only adjacent constant states interact and thus may be solved "exactly" for one time step. This exact solution at

time t_{n+1} is then averaged over each cell to produce the numerical approximation u_j^{n+1}, i.e.,

$$u_j^{n+1} = \frac{1}{\Delta x} \int_{x_{j-1/2}}^{x_{j+1/2}} u(x; \Delta t)\, dx.$$

Using the divergence theorem, the scheme can be put in conservation form with $g_{j+1/2} = H(u(x_{j+1/2}, 0^+))$. In other words, the numerical flux is the same as the physical flux applied to the exact solution of the Riemann problem Eq. (3.4), with initial data

$$u(x, 0) \equiv u_j^n, \; x \leqslant x_{j+1/2} \qquad u(x, 0) \equiv u_{j+1}^n, \; x > x_{j+1/2}.$$

We label this flux function $g_{\mathrm{GOD}}(u_j^n, u_{j+1}^n) \equiv g_{j+1/2}^n$. This is clearly an "upwind" difference scheme in the sense that, if $H' > 0$, then $g_{j+1/2} = f(u_j)$, likewise, if $H' < 0$, then $g_{j+1/2} = f(u_{j+1})$. Another formulation of the above flux function [27] is simply that

$$g_{\mathrm{GOD}}(u_j, u_{j+1}) = \chi_{j+1/2} \min[\chi_{j+1/2}, H(u)],$$

where the minimum is taken over the interval $[\min(u_j, u_{j+1}), \max(u_j, u_{j+1}))$ and $\chi_{j+1/2} = \mathrm{sgn}(u_{j+1} - u_j)$.

There are other useful upwind monotone schemes, see [27], which, while powerful in their own right, do not easily extend to several dimensions and thus are severely limited. We now present a new upwind monotone scheme (HJ), for the particular case when

$$H(u) = f(u^2)$$

with $f'(u) < 0$. Define

$$g_{\mathrm{HJ}}(u_j^n, u_{j+1}^n) = f((\min(u_j^n, 0))^2 + (\max(u_{j+1}^n, 0))^2). \tag{3.7}$$

The advantage to this scheme is that it easily generalizes to several space dimensions (see below).

It is a simple matter to put any of these schemes in terms of the Hamilton–Jacobi variable ψ. The numerical flux g approximates H. In the shock formulation, g must be differentiated (Eqs. (3.4), (3.5)). However, H (and hence its numerical approximation g) appears directly in the Hamilton–Jacobi formulation (Eq. (3.1)), thus we may immediately write

$$\Psi_j^{n+1} = \Psi_j^n - \Delta t\, g(D_- \Psi_j^n, D_+ \Psi_j^n).$$

Here, g is any of the above numerical fluxes. (In the Hamilton–Jacobi context, it is natural to thus refer to g as the numerical Hamiltonian, and we shall now do so). We note that the CFL condition is $g_{\mathrm{HJ}}\, (\Delta t/\Delta x)|H'| \leqslant 1/2$.

(2) *Higher Order Schemes for One Space Dimension*

Although monotone schemes have the desirable properties of conservation form, no spurious oscillations, and an entropy limit, they are unfortunately limited to first order and smear out most discontinuities. However, they do suggest other kinds of schemes of higher accuracy that retain these properties.

One new class of higher order accurate algorithms was devised for conservation laws in [13, 14]. They rely on an essentially non-oscillatory interpolant (and are thus called "ENO" schemes) and can be constructed to arbitrary high order. In fact, viewing them in the Hamilton–Jacobi framework results in substantial simplification; thus we proceed directly to this setting.

The idea is as follows. Consider the solution to $\psi_t + H(\psi_x) = 0$, with ψ given at $t = t^n$. We integrate this in time from $t = t^n$ to $t = t^{n+1}$ for any fixed x and arrive at

$$\psi(x, t^{n+1}) = \psi(x, t^n) - \int_0^{\Delta t} H(\psi_x(x, t^n + s))\, ds.$$

To approximate this procedure, let Ψ_j^n approximate the exact solution at time $n\,\Delta t$. We want to devise a function $R^M(x; \Psi^n)$ which approximates $\psi(x, t^n)$ in regions of smoothness of ψ, up to $O(\Delta x)^{M+1}$. Moreover, this approximating function should be non-oscillatory even if ψ_x is discontinuous, i.e., no new significant oscillations are introduced. We build the interpolants from the ground up as follows. For $M = 1$, $R^1(x; \Psi^n)$ is defined to be the unique piecewise linear function connecting the points (x_v, Ψ_v^n), thus producing precisely Godunov's first-order algorithm. For $M = 2$, in each cell $x_j \leqslant x \leqslant x_{j+1}$, $R^2(x; \Psi^n)$ is the parabola passing through $(x_j; \Psi_j^n)$, (x_{j+1}, Ψ_{j+1}^n), and whichever point (x_{j-1}, Ψ_{j-1}^n) (on the left) or (x_{j+2}, Ψ_{j+2}^n) (on the right) yields the smallest (in magnitude) second derivative, thus limiting oscillations. We store this choice and repeat inductively for more accuracy; that is, a cubic is obtained using the three points for the parabola, and an additional point, either just to the left or to the right, whichever yields a smaller magnitude third derivative. (The general M degree construction may be found in Appendix B). This procedure creates a function which (1) interpolates Ψ_v^n at $M+1$ consecutive points containing x_j and x_{j+1} and (2) minimizes the magnitude of all derivatives, given the above constraint. It can be shown (see [14]) that, if $\psi(x)$ is piecewise C_0^∞, has at most a finite number of isolated jumps in its derivatives and is smooth at $x = x_0$, then for Δx sufficiently small,

$$\left[\left(\frac{d}{dx}\right)^v \psi(x) - \left(\frac{d}{dx}\right)^v R^M(x; \psi)\right]_{x = x_0} = O(\Delta x)^{M-v+1},$$

where $v = 0, 1, 2, \ldots M$. The global statement is also true, namely,

$$\mathrm{TV}\left[\frac{d}{dx} R^M(x; \psi)\right] \leqslant \mathrm{TV}\left[\frac{d}{dx}\psi(x)\right] + O(\Delta x)^M,$$

where TV is the total variation of a BV function as defined in [17]. To continue the algorithm, we then solve the initial value problem (Eq. (3.1)), with $\Psi(x, 0) = R^M(x; \Psi^n)$, either exactly (as in the Godunov scheme) or approximately, using any other monotone approximation. To obtain the new Ψ^{n+1}, we define

$$\Psi_j^{n+1} = \int_0^{\Delta t} \Psi_t(x_j, s)\, ds + \Psi_j^n = \Psi_j^n - \int_0^{\Delta t} H(\Psi_x(x_j, s))\, ds,$$

where Δt is taken small enough so that only waves from adjacent cells interact.

We simplify this method for our calculations. First, instead of solving the exact problem, we approximate the Godunov flux by the simpler monotone flux g_{HJ}. The numerical time integration can be performed either by formally replacing higher time derivatives to arbitrary order by space derivatives, see [13], or by producing a non-oscillatory Runge–Kutta type algorithm [29] from the semi-discrete formulation

$$\frac{\partial}{\partial t}\Psi_j = -g_{\mathrm{GOD}}\left(\frac{d}{dx}R^N(x_j^-; \Psi), \frac{d}{dx}R^N(x_j^+; \Psi)\right).$$

We note that for first-order monotone approximations to a linear equation $u_t = -u_x$, the Hamilton–Jacobi and conservation law formulations yield the same schemes. However, differences occur for higher order methods. A second-order approximation for conservation form gives

$$\frac{\partial u_j}{\partial t} = -D_-\left[u_j + \frac{\Delta x}{2} m[D_- u_j, D_+ u_j]\right]$$

and

$$\frac{\partial \Psi_j}{\partial t} = -\left[D_- \Psi_j + \frac{\Delta x}{2} m[D_- D_- \Psi_j, D_- D_+ \Psi_j]\right]$$

for Hamilton–Jacobi form (m is defined below). The first is only first-order accurate near critical points because the term with $m[\ ]$ gives $u_x + O(\Delta x)$, and the coefficient in the $O(\Delta x)$ is not Lipschitz continuous near these points. The second is uniformly second-order accurate since the analogous term yields $\Psi_{xx} + O(\Delta x)$. We also have estimates

$$\frac{\partial}{\partial t}\sum |D_+ u_j| \leqslant 0, \qquad \frac{\partial}{\partial t}\sum |D_+ D_- \Psi_j| \leqslant 0.$$

B. *Several Dimensions*

In general, the Hamilton–Jacobi equations in several dimensions cannot be recast as a simple system of conservation laws. However, using information gleaned from the one-dimensional correspondence and resulting scheme design, we may now con-

struct a new class of monotone upwind schemes for arbitrary H in several space dimensions. In our application here, namely the case $H(\psi_{x_1}, ..., \psi_{x_N}) = f(\psi_{x_1}^2, ..., \psi_{x_N}^2)$, where f is non-increasing in each of its arguments, we devise a particularly simple class of algorithms.

(1) *First-Order Schemes for Several Dimensions*

Crandall and Lions [5] have analyzed monotone (and hence first-order) difference approximations to the Hamilton–Jacobi equations. As an introduction, we consider the two-space dimension discrete approximation

$$\Psi_{j,k}^{n+1} = \Psi_{j,k} - \Delta t g(D_+^x \Psi_{j-p,k-r}, ..., D_+^x \Psi_{j+q,k+s+1}; D_+^y \Psi_{j-p,k-r}, ..., D_+^y \Psi_{j+q+1,k+s}), \tag{3.8}$$

where $p, q, r, s \geqslant 0$, and g is thus a function of $(p+q+1)(r+s+1)$ variables. Consistency requires that g be Lipshitz continuous and that $g(a, ..., a; b, b, ..., b) = H(a, b)$. Crandall and Lions proved a rate of convergence result of $O(\Delta t)^{1/2}$ in the max norm. Their only example, however, is Lax–Friedrichs, which relys on a central difference formulation and suffers from excessive diffusion. Unfortunately, in our solution of front propagation problems, the computational domain must be limited to a finite region, and thus far-field boundary conditions are required. A central difference scheme creates spurious waves at the boundary because it does not make use of the direction of propagating characteristics. In fact, an original attempt to solve the level surface Hamilton–Jacobi equation (Eq. (2.13)) using Lax–Friedrichs suffered from just this problem, and is what ultimately led to the introduction of upwind schemes.

We begin by defining a new upwind first-order generalization of Godunov's scheme [12, 27]. Let

$$\chi_{jk}^{(x)} = \operatorname{sgn}[D_+^x D_-^x \Psi_{jk}], \qquad \chi_{jk}^{(y)} = \operatorname{sgn}[D_+^y D_-^y \Psi_{jk}].$$

Define

$$H_{jk}(u) = \chi_{jk}^{(y)} \min(\chi_{jk}^{(y)} H(u, v)) \quad v \in [\min(D_-^y \Psi_{jk}, D_+^y \Psi_{jk}), \max(D_-^y \Psi_{jk}, D_+^y \Psi_{jk}))). \tag{3.9}$$

Then this Hamilton–Jacobi–Godunov scheme has numerical Hamiltonian

$$g_{\mathrm{GOD}}(D_-^x \Psi_{jk}, D_+^x \Psi_{jk}, D_-^y \Psi_{jk}, D_+^y \Psi_{jk}) = \chi_{jk}^{(x)} \max(\chi_{jk}^{(x)} H_{jk}(u)), \quad u \in [\min(D_-^x \Psi_{jk}, D_+^x \Psi_{jk}), \min(D_-^x \Psi_{jk}, D_+^x \Psi_{jk})). \tag{3.10}$$

This is fully upwind, in that, if $\partial H/\partial u < 0$, $\partial H/\partial v < 0$, then the scheme looks in the proper direction, i.e., $g_{\mathrm{GOD}} = H(D_+^x \Psi_{jk}; D_+^y \Psi_{jk})$. The same holds for the other three cases, and the numerical Hamiltonian g does not depend on the ordering of the operators. In fact, the scheme is monotone if $1 \geqslant \Delta t/\Delta x\, |H_1| + \Delta t/\Delta y\, |H_2|$. Near

sonic points, i.e., points where $\partial H/\partial u$ or $\partial H/\partial v$ vanish, the Hamiltonian defined in Eq. (3.9) becomes a bit complicated, and we resist reproducing the formula here.

In our special case $H(u, v) = f(u^2, v^2)$, with f non-increasing in both variables, our one-dimensional HJ scheme is easily extended to two dimensions through

$$g_{\mathrm{HJ}} = f(((\min(D^x_- \Psi_{jk}, 0))^2 + (\max(D^x_+ \Psi_{jk}, 0))^2), ((\min(D^y_- \Psi_{jk}, 0))^2 + (\max(D^y_+ \Psi_{jk}, 0))^2)) \tag{3.11}$$

which is fully upwind and monotone, subject to the CFL restriction $1 \geqslant 2[(\Delta t/\Delta x)\,|H_1| + (\Delta t/\Delta y)\,|H_2|]$.

(2) *Higher Order Schemes for Higher Dimensions*

We extend our higher order methods to higher dimensions by using the spatially discrete temporally continuous formulation obtained from our one-dimensional ENO reconstruction procedure dimension by dimension. Thus, for example, a second order in space method is

$$\frac{\partial}{\partial_t} \Psi_{jk} = -g\Big[D^x_- \Psi_{jk} + \frac{\Delta x}{2} m[D^x_- D^x_+ \Psi_{jk}, D^x_- D^x_- \Psi_{jk}],$$

$$D^x_+ \Psi_{jk} - \frac{\Delta x}{2} m[D^x_+ D^x_+ \Psi_{jk}, D^x_+ D^x_- \Psi_{jk}];$$

$$D^y_- \Psi_{jk} + \frac{\Delta y}{2} m[D^y_- D^y_+ \Psi_{jk}, D^y_- D^y_- \Psi_{jk}],$$

$$D^y_+ - \frac{\Delta y}{2} m[D^y_+ D^y_+ \Psi_{jk}, D^y_+ D^y_- \Psi_{jk}]\Big],$$

where $m[x, y] = x$ if $|x| \leqslant |y|$ and $m[x, y] = y$ if $|x| > |y|$. There is no loss of the desirable properties if m is defined as above except if $xy < 0$ in which case it is taken to be zero. We shall use this definition in the next section, since it yields a "smoother" flux function.

To obtain a fully discrete algorithm of the appropriate accuracy in time, we view Eq. (3.12) as a nonlinear evolution operator of the type

$$\frac{\partial}{\partial t} \Psi_{jk} = -L[\Psi, j, k]$$

and employ certain Runge–Kutta type shemes (see [29] for a theoretical justification). For example, a second-order essentially non-oscillatory Runge–Kutta algorithm is

$$\bar{\Psi}^{n+1}_{jk} = \Psi^n_{jk} - \Delta t\, L[\Psi^n, j, k]$$

$$\Psi^{n+1}_{jk} = 1/2\Psi^n_{jk} + 1/2\bar{\Psi}^{n+1}_{jk} - \frac{\Delta t}{2} L[\bar{\Psi}^{n+1}, j, k],$$

which has a slightly reduced CFL restriction from the underlying monotone algorithm.

C. *General $F(K)$*

For general $F(K)$, we have

$$\psi_t + F(K)H(\nabla\psi) = 0, \tag{3.13}$$

where K is the curvature and involves terms like $\psi_{xx}, \psi_{yy}, \psi_{xy}$. We have found that it is necessary to separate $F(K)$ into a constant term (the convection part) and those terms dependent on K, that is, $F(K) = F_0 + F_1(K)$, where F_0 is a constant (possibly zero) and $F_1(0) = 0$. Equation (3.13) then becomes

$$\psi_t + (F_0)H(\nabla\psi) = -F_1(K)H(\nabla\psi). \tag{3.14}$$

While the convection term $H(\nabla\psi)$ on the left is approximated using one of our non-oscillatory upwind methods, all derivatives on the right, including $\nabla\psi$, are approximated by central differences. The reason for this may easily be seen from the following illustration: Consider a circular front of initial radius one moving with speed $F(K) = -K$. In Formulation (2) (Eqs. (3.1), (3.3)), this is one of an infinite number of concentric level curves; those with small radii near the center have large curvatures. Since the term $-KH(\nabla\psi)$ on the right depends on multiplication and division by $(\psi_x^2 + \psi_y^2)^{1/2}$, which is very close to zero near the origin, the approximation to ψ_x and ψ_y must be the same within K and $H(\nabla\psi)$, otherwise, large errors result. Thus, it is simplest to maintain central differences throughout the right-hand side. One can also show linear stability of this semi-discrete approximation. We make this spatially discrete algorithm fully discrete using either just a forward Euler time discretization (first-order accurate) or a higher order Runge–Kutta procedure, as in [29]. Because of the "parabolic" right-hand side, any such method will have a somewhat smaller CFL restriction than the "inviscid" approximation.

D. *Initialization and Singularities*

For propagating level surfaces, we initialize ψ by taking $\psi(\bar{x}, 0) = 1 \pm d^2$, where d is the distance from the point $\bar{x}$ to the initial surface, and the plus (minus) sign is chosen if $\bar{x}$ is inside (outside) the initial surface.

There will be points where $\nabla\psi$ vanishes. On the right-hand side of Eq. (3.14), division by zero then occurs in the denominator of the curvature evaluation (N.B., this does not happen in the functional representation (Formulation (1)). Given the above initialization function, to a first approximation such points are surrounded by spherical level surfaces, and we may formally evaluate the limit $F_1(K)\nabla\psi$ as the radius of the concentric level spheres goes to zero. If a mesh point falls exactly on a critical point of ψ, this limit is employed directly into the scheme at that point.

E. *Far-Field Boundary Conditions*

In the case of a propagating function (Formulation (1), Eqs. (3.1)–(3.2)), if $\psi_x(x, 0) = 0$ at x_1 and x_2 (using one dimension as an example), then we can employ symmetric boundary conditions at each end. However, in the level surface case (Formulation (2), Eqs. (3.1), (3.3)), Eq. (3.1) must be initialized and solved for all R^N. Thus the computational domain must be truncated. With a positive convection term S in Eq. (3.14), characteristcs will head outwards far from the region of interest, and our upwind schemes are perfectly suited for these problems. In first-order schemes, no far field numerical boundary conditions are needed for the convection term, since the schemes "look" in the right direction. Higher order schemes involve a choice of directions in order to remove spurious oscillations, thus we replace $m[D_-^x D_+^x \Psi_j, D_-^x D_-^x \Psi_j]$ with the second-order term $D_-^x D_-^x \Psi_j$, at the right-hand far-field boundary, etc.

However, the curvature term on the right-hand side of Eq. (3.14) must be treated with some care. If the convection term is relatively large, instabilities in this approximation will be swept out of the domain. However, if $F_0 = 0$, the boundary plays a role. If the boundary is far from the initial surface, we may imagine that the level surface passing through each boundary point is almost a sphere. Thus, we use the exact solution to the collapsing sphere as the far-field boundary condition to the right-hand side of ϕ_t.

F. *Addition of Passive Advection*

Suppose the propagating front is also passively advected by an underlying velocity field $\bar{U} = (u_1, ..., u_N)$ in N-dimensional domain space. It can be shown that Eq. (3.13) becomes

$$\psi_t + F(K)H(\nabla\psi) + \bar{U} \cdot \nabla\psi = 0. \tag{3.15}$$

Here, of course, $\bar{U}$ may depend on x and t. For the numerical results in the next

$$u_i \frac{\partial \psi}{\partial x_i} \approx u_i^+ D_- \psi_i + u_i^- D_+ \psi_i.$$

However, when $\bar{U}$ depends on ψ, the front moves itself in a non-local manner, and more sophisticated methods are required. We will report on the extension of our algorithms to this important problem elsewhere [36].

IV. Moving Curves

In this section, we demonstrate the versatility of our PSC algorithms applied to a variety of test problems involving moving curves in a plane. We use the first and

second-order Hamilton–Jacobi schemes applied to both propagating functions and level curves. In all of these examples, the only input parameters are the initial curves, the time step $\Delta t = 1/N_{\text{point}}$ (we use the size space step in each coordinate direction), the order of the scheme and the speed function $F(K)$. Everything else is handled automatically by the Hamilton–Jacobi formulation.

A. $F(K) = 1 - \varepsilon K$, *Propagating Function, Dependence on* ε

First, we show the effect of the curvature term on the formation of singularities in the propagating fronts. Consider the initial curve $\psi(x, 0) = \cos 8\pi x$, $0 \leqslant x \leqslant 1$. Using these initial data, we compute the solution to the initial value problem (Eq. (3.1), (3.2)) with our second-order Hamilton–Jacobi scheme and $F(K) = 1 - \varepsilon K$, where $K = -\psi_{xx}/(1 + \Psi_x^2)^{3/2}$. Thus, the "peaks" move slower than the "troughs." Periodic boundary conditions are employed in this scheme. In Figs. 1a ($\varepsilon = 0.0$), 1b ($\varepsilon = 0.25$), and 1c ($\varepsilon = .1$), we graph the position of the front at various times. There are $N_{\text{point}} = 160$ mesh points in the unit interval with time step $\Delta t = 0.001$. In the case $\varepsilon = 0$ (Fig. (1a), corners form in the moving front, and these "shocks" propagate upwards. In the case $\varepsilon = 0.025$ (Fig. 1b), the front stays smooth due to

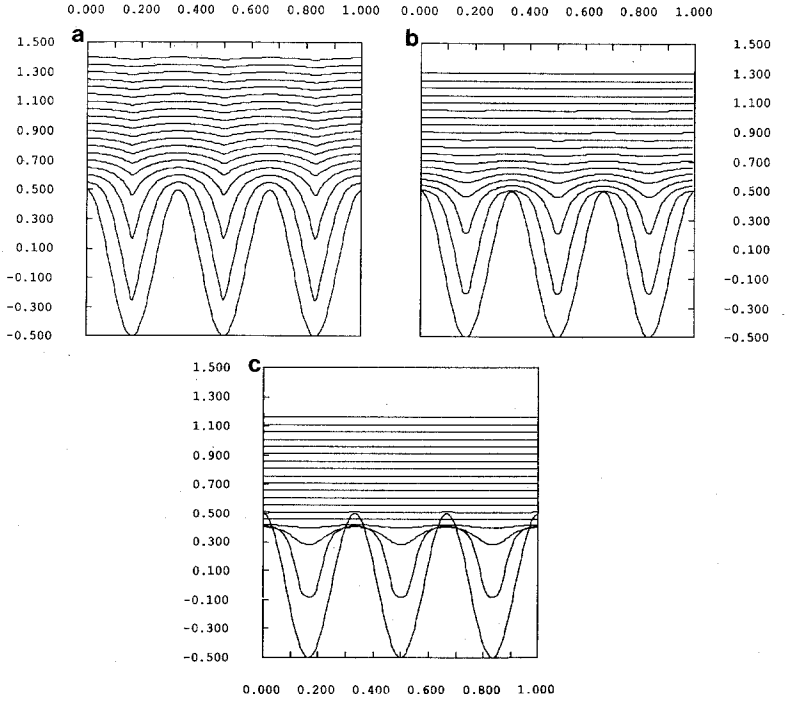

FIG. 1. Propagating initial cosine curve: $F(K) = 1 - \varepsilon k$. Plots of ψ vs x. All plots at $T = 0.0$, 0.9 (0.05): (a) $F(K) = 1 - \varepsilon K$, $\varepsilon = 0.0$; (b) $F(K) = 1 - \varepsilon K$, $\varepsilon = 0.025$; (c) $F(K) = 1 - \varepsilon K$, $\varepsilon = 0.1$. $\psi(x, 0) = \cos(8\pi x)$.

TABLE I

Determination of Order of Hamilton–Jacobi Schemes

Actual order of Hamilton–Jacobi schemes		
Mesh size	"First" order	"Second" order
$h = 0.01/10$	$R = 1.0025$	$R = 2.2144$
$h = 0.01/20$	$R = 1.0475$	$R = 1.8581$
$h = 0.01/40$	$R = 1.1000$	$R = 1.8994$
$h = 0.01/80$	$R = 1.2225$	$R = 2.0369$
$h = 0.01/160$	$R = 1.5850$	$R = 2.3084$

the curvature term. In the case $\varepsilon = 0.1$ (Fig. 1c), diffusion is so large that the peaks first start moving downwards ($1 < \varepsilon K < 0$) before they flatten out enough to propagate upwards.

B. *Error Analysis*

We wish to verify that our Hamilton–Jacobi schemes are indeed first and second order. We consider initial data $\psi(x, 0) = \cos 2\pi x$, $0 \leqslant x \leqslant 1$, $F(K) = 1 - \varepsilon K$, $\varepsilon = 0.01$ and compute the solution $u_h(x, t)$ to Eqs. (3.1)–(3.2) for $h = 0.01/2^p$, $\Delta t = 0.005/2^p$, $p = 0, 1, 2, 3, 4, 5, 6$. If we assume that the exact solution $v(x, t)$ can be written as

$$v(x, t) = u_h(x, t) + Ch^R + O(h^{R+1}),$$

then we can estimate the order R of the method by

$$2^R = \frac{v - u_h}{v - u_{h/2}}.$$

Since we do not know the exact solution, we approximate v by the most accurate calculation. In Table I, we give the value of R found by comparing u_h and $u_{h/2}$ for various values of h at time $t = 1.0$, using $u_{h=1/6400}$ ($p = 6$) as the exact solution. Here, errors are measured using the discrete L^2 norm. The schemes are roughly of at least first and second order, as predicted by the theory. Although the results appear a little better than that, we hesitate to draw any conclusions.

C. $F(K) = -K$, *Propagating Functions*

We consider a periodic curve $\psi(x, 0) = \sin 2\pi x$ as initial data, $F(K) = -K$, and solve Eqs. (3.1)–(3.2) using our second-order Hamilton–Jacobi scheme. This corresponds to a curve moving under its curvature. This problem has been studied extensively in [7–10] and reduces to a relatively straightforward parabolic equation. We use 160 mesh points per side and a time step $\Delta t = 0.001$. In Fig. 2, we

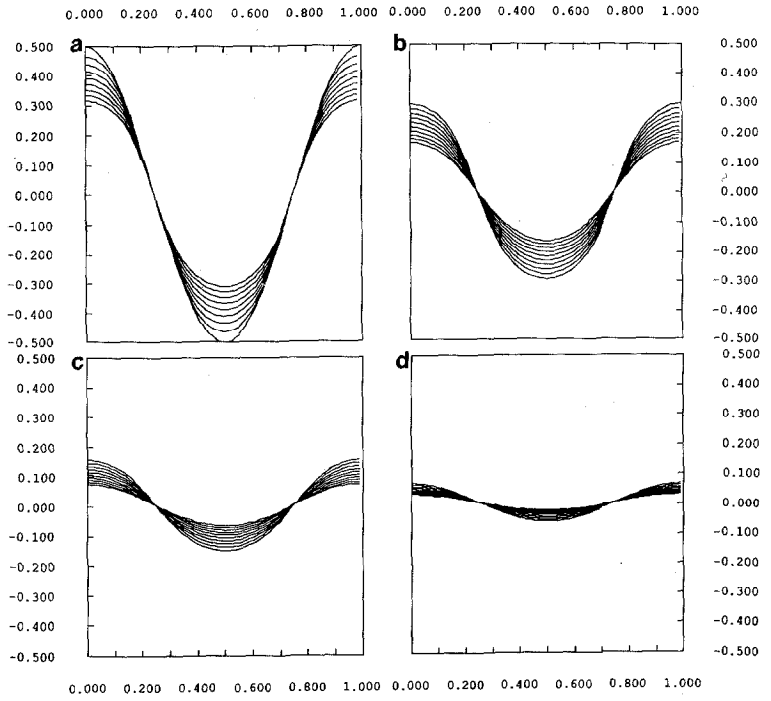

FIG. 2. Propagating initial sine curve: $F(K) = -K$. Motion under curvature: Plots of ψ vs. x. (a) $F(K) = -K$, Plots at $= 0.0, 0.5$ (0.05); (b) $F(K) = -K$, Plots at $T = 0.5, 1.0$ (0.05); (c) $F(K) = -K$, Plots at $T = 1.0, 1.5$ (0.05); (d) $F(K) = -K$, Plots at $T = 1.5, 2.0$ (0.05). $\psi(x, 0) = \sin(2\pi x)$.

draw the front at various times, demonstrating that the periodic front relaxes to a straight line with increasing time.

D. *Level Curve, Burning out, Development of Corners*

We consider a seven-pointed star

$$\gamma(s) = (0.1 + (0.065 \sin(7 \cdot 2\pi s)(\cos(2\pi s), \sin(2\pi s)), \qquad s \in [0, 1]$$

as the initial curve and solve Eqs. (3.1), (3.3) with $F(K) = 1$, using the initialization given in Section III.D. The computational domain is a square centered at the origin of side length $\frac{1}{2}$. We use 300 mesh points per side, time step $\Delta t = 0.0005$ and the second-order Hamilton–Jacobi scheme. Thus, we are following an entire family of star-shaped regions lying on a higher dimensional surface. At any time $n\,\Delta t$, the front itself is plotted by passing the discrete grid function Ψ_{ij}^n to a standard contour plotter and asking for the contour $\Psi = 1$. The initial curve corresponds to the boundary of the shaded region, and the position of the front at various times is shown in Fig. 3. The smooth initial curve develops sharp corners which then open up as the front burns, asymptotically approaching a circle.

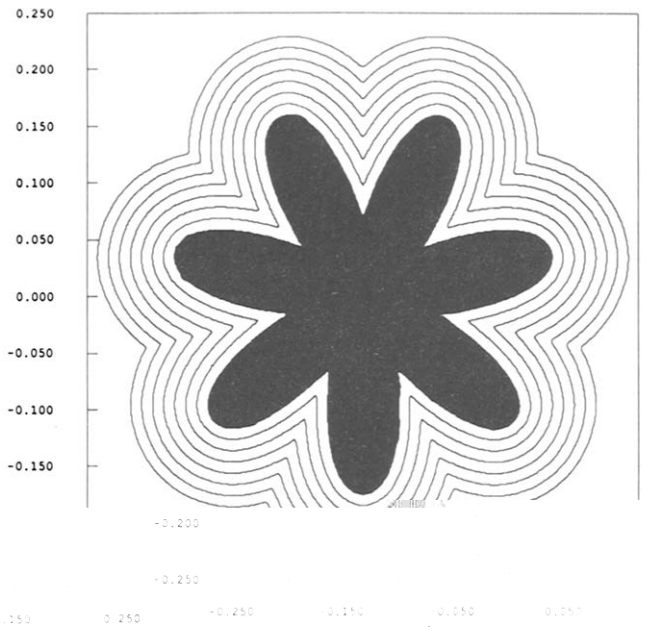

FIG. 3. Star-shaped front burning out: $F(K) = 1$, $T = 0.0, 0.7\ (0.01)$.

E. *Level Curve, Motion under Curvature*

With the same initial curve as Example IV.D above, we let $F(K) = -K$, corresponding to a front moving in with speed equal to its curvature. It has recently been shown [10] that any non-intersecting curve must collapse smoothly to a circle under this motion. With $N_{\text{point}} = 300$, and $\Delta t = 0.0005$, in Fig. 4a, we show the front at time $t = 0.0, 0.01, 0.02, 0.03, 0.04, 0.05$. We use the second-order Hamilton–Jacobi scheme. Here, we have scaled time by a factor of 100, because the real front moves so quickly. In Figs. 4a–d we show the continued evolution of the surface from $t = 0.0$ to $t = 0.2$. The plots show the relaxation of the peaks and troughs and the smoothing into a circle. In Fig. 5, we show the results of the same motion applied to a different initial curve, namely the wound spiral traced out by

$$\gamma(s) = (0.1e^{(-10y(s))} - (0.1 - x(s))/20)(\cos(a(s)), \sin(a(s))),$$

where $a(s) = 25 \tan^{-1}(10y(s))$ and

$$x(s) = (0.1)\cos(2\pi s) + 0.1,\ y(s) = (0.5)\sin(2\pi s) + 0.1, \qquad s \in [0, 1].$$

With $N_{\text{point}} = 200$ and $\Delta t = 0.0001$ we use the second-order scheme. Again, we stress that we are following a entire family of concentric initial spirals. Figure 5a shows the unwrapping of the spiral from $t = 0$ and $t = 0.65$. In Figs. 5a–d we show the

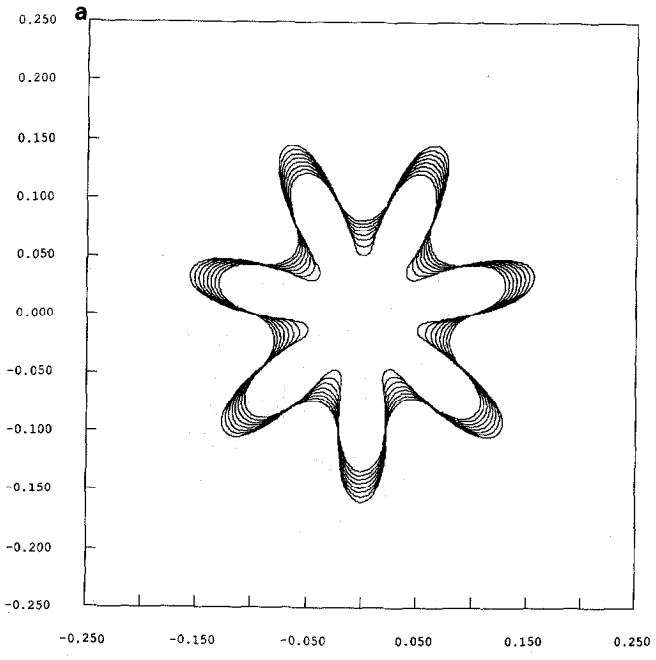

FIG. 4a. Star-shaped curve collapsing under curvature (Beginning): $F(K) = -K$, $T = 0.0, 0.5\ (0.005)$.

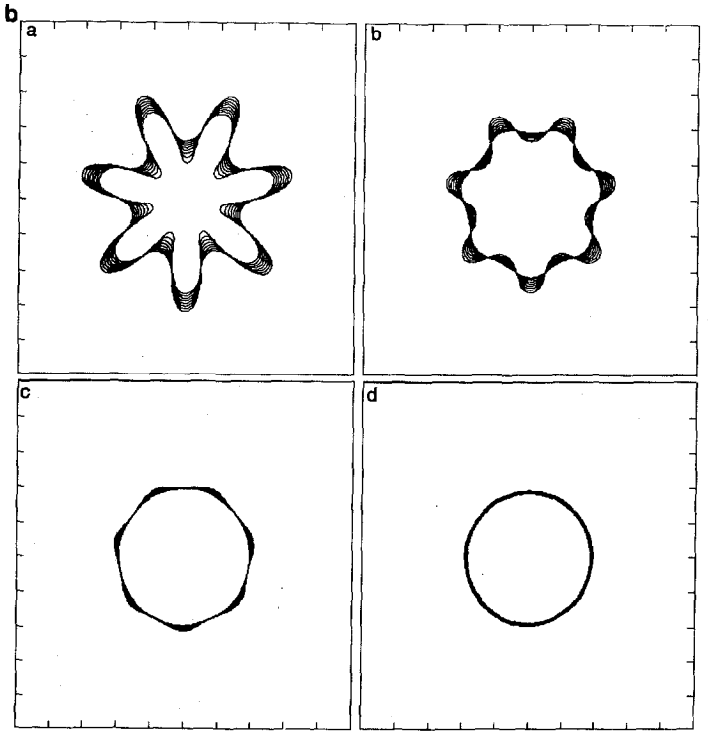

FIG. 4b. Star-shaped curve collapsing under curvature (Continued) $F(K) = -K$: (a) $T = 0.0, 0.5$ (0.005); (b) $T = 0.5, 1.0$ (0.005); (c) $T = 1.0, 1.5$ (0.005); (d) $T = 1.5, 2.0$ (0.005).

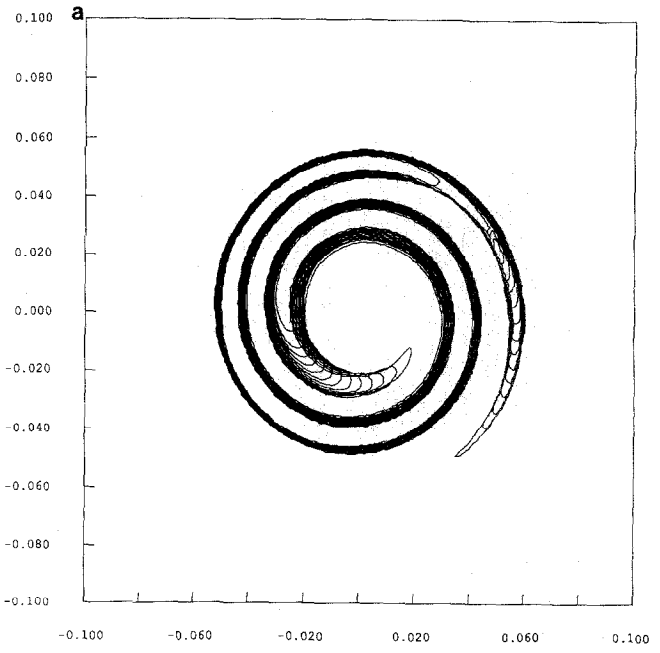

FIG. 5a. Wound spiral collapsing under curvature (Beginning): $F(K) = -K$, $T = 0.0, 0.065$ (0.005).

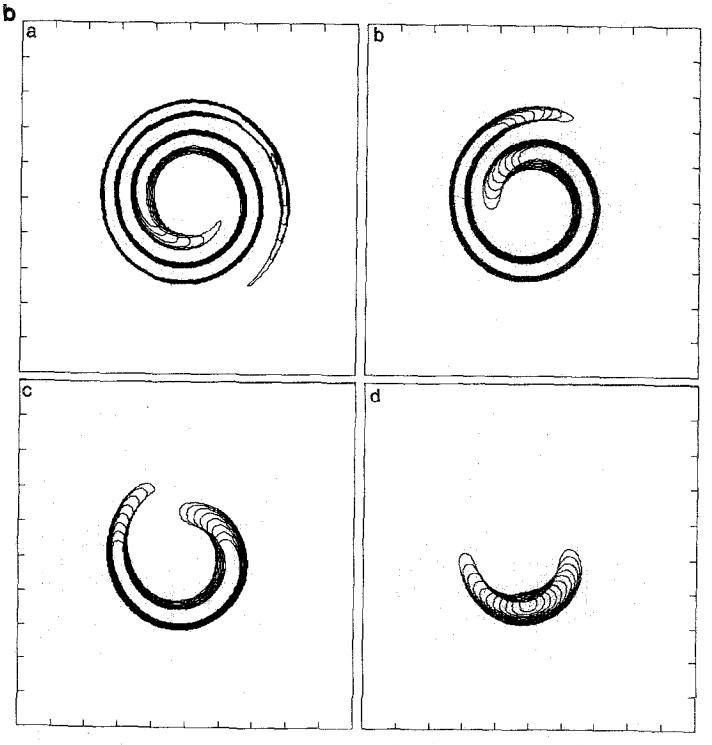

FIG. 5b. Wound spiral collapsing under curvature (Complete history) $F(K) = -K$: (a) $T = 0.0, 0.065$ (0.01); (b) $T = 0.065, 0.130$ (0.01); (c) $T = 0.130, 0.195$ (0.01); (d) $T = 0.195, 0.295$ (0.01).

collapse to a circle and eventual disappearance at $t = 0.295$. (The surface vanishes when $\Psi_{ij}^n < 1$ for all ij.)

F. *Level Curve, $F(K) = 1 - \varepsilon K$, Merging and Breaking*

Using the wound spiral initial curve in the above example, Fig. 6 shows the results with $F(K) = 1 - \varepsilon K$, $\varepsilon = 0.01$, $N_{\text{point}} = 200$, and $\Delta t = 0.0001$. Again, we use the second-order Hamilton–Jacobi scheme. Figure 6a shows the initial curve as the boundary of the shaded region. In Fig. 6b, the spiral expands and pinches off due to the strong convection component, separating into two curves, one propagating outwards and one shrinking in. In Fig. 6c, the front at $t = 0.04$ is the boundary of the shaded region. The outer front expands and the inner front collapses and disappears. In Fig. 6d, all that remains is the outer front which asymptotically approaches a circle.

G. *Level Curve, Passive Advection, and Propagation*

Finally, we solve the passive advection plus propagation equation (Eq. (3.15)) with the initial seven-pointed star in Example D, $F(K) = 1$, and

$$\bar{U} = (u_1(x, y, t), u_2(x, y, t)) = (-y, x)(100(x^2 + y^2)).$$

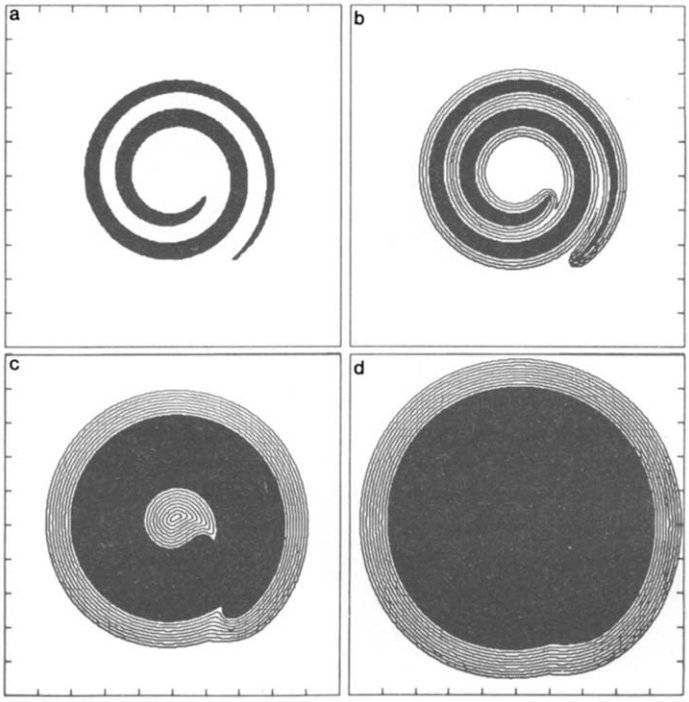

FIG. 6. Burning spiral: merging and breaking $F(K) = 1 - \varepsilon K$, $\varepsilon = 0.01$: (a) $T = 0.0$ (initial curve); (b) $T = 0.00$, 0.03 (0.01); (c) $T = 0.04$, 0.12 (0.01); (d) $T = 0.13$, 0.22, (0.01).

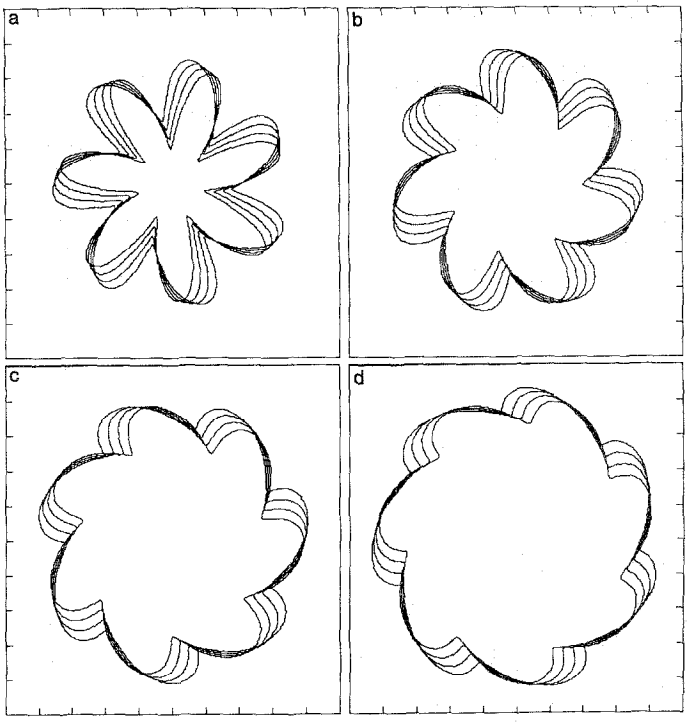

FIG. 7. Passive advection and propagation: $F(K) = 1 +$ Rotation: (a) $T = 0.0$, 0.03 (0.01); (b) $T = 0.03$, 0.06 (0.01); (c) $T = 0.06$, 0.09 (0.01); (d) $T = 0.09$, 0.12 (0.01).

This corresponds to solid body counterclockwise rotation around the origin with tangential velocity 1 along the circle with radius 0.1 centered at the origin. The size of the numerical parameters and scheme order are the same as in Example D. In Fig. 7, we show the expanding and spinning star at various times.

V. MOVING SURFACES

In this section, we use PSC algorithms to compute the evolution of several two-dimensional surfaces in three space dimensions. We use the initializing function given in Section III.D and the first-order Hamilton-Jacobi scheme given in Eq. (3.11).

A. *Propagating Function Surfaces*, $F(K) = 1$, $F(K) = 1 - \varepsilon K$, $F(K) = K$

We evolve the initial surface

$$\psi(x, y, 0) = -0.25[\cos(2\pi x) - 1][\cos(2\pi y) - 1] + 1$$

according to Eqs. (3.1), (3.2), with $F(K) = 1$, $\Delta t = 0.01$, $N_{\text{point}} = 50$ (in each direction), and periodic boundary conditions. This surface is flat in the boundary of the unit square centered at the origin and has a global minimum at (0, 0). In Fig. 8a, we plot the surface at various times, showing the focusing of the minimum into a deep dent which then opens up. The surface moves upward with unit speed asymptotically approaching a flat sheet. Next, we add curvature effects to the speed function and let $F(K) = 1 - \varepsilon K$, $\varepsilon = 0.1$. The time step is reduced to $\Delta t = 0.0001$ because of stability requirements from the addition of a parabolic term. In Fig. 8b, we plot the surface at various times. Here, the dent is greatly smoothed due to the curvature effects, and the surface becomes flat much faster, similar to the one-dimensional case (Fig. 1).

We then consider a saddle surface, described by

$$\psi(x, y, 0) = \cos(2\pi x) - \cos(2\pi y).$$

Again, we start with $F(K) = 1$, $\Delta t = 0.01$, $N_{\text{point}} = 50$, and periodic boundary conditions. In Fig. 9a, we plot the surface at various times. Here, the rising surface develops a discontinuity passing through the saddle point in the y coordinate direction, corresponding to a shock in the tangent vector. Adding curvature (Fig. 9b, $F(K) = 1 - \varepsilon K$, $\varepsilon = 0.1$), the shock is smoothed out, and the surface smoothly approaches a flat sheet.

Finally, we move the saddle surface purely under its own curvature ($F(K) = -K$, where K is the mean curvature). In Fig. 10, we show the front at various times and show the rapid motion toward the steady state flat sheet.

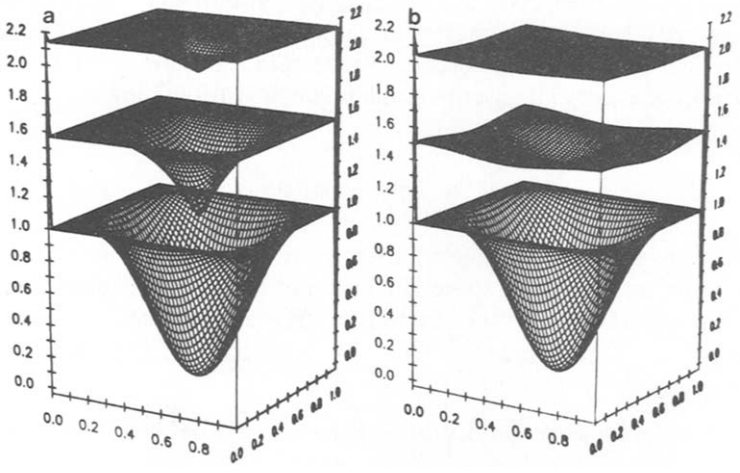

FIG. 8. Propagating surface: $F(K) = 1 - \varepsilon K$, mean curvature: (a) $F(K) = 1$, surface at $T = 0.0, 0.3, 0.6$; (b) $F(K) = 1 - \varepsilon K$, $\varepsilon = 0.1$, surface at $T = 0.0, 0.3, 0.6$.

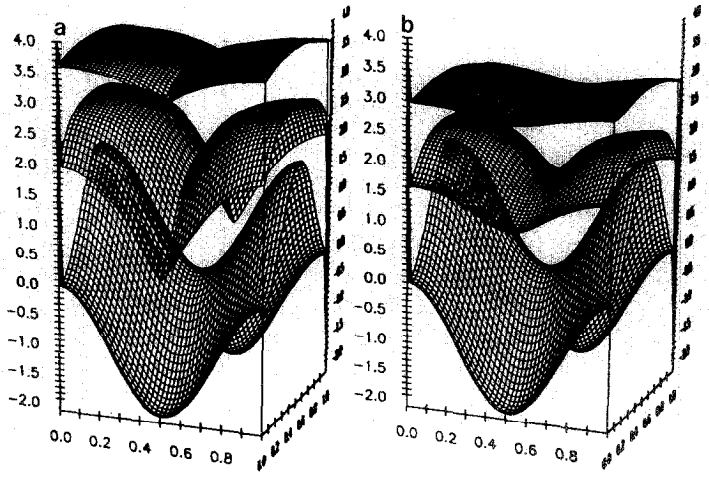

FIG. 9. Propagating surface: $F(K) = 1 - \varepsilon K$, mean curvature: (a) $F(K) = 1$, surface at $T = 0.0, 0.3, 0.6$; (b) $F(K) = 1 - \varepsilon K$, $\varepsilon = 0.1$, surface at $T = 0.0, 0.3, 0.6$.

B. *Level Surface, Sphere,* $F(K) = 1$, *Mean Curvature*

We evolve the initial surface described by the sphere of radius 0.5. We initialize $\psi^n_{i,j,k}$ using the distance function, as described in III.D; in this case, the distance function from the initial surface may be analytically expressed. The computational domain is a rectangular parallelpiped with lower front left corner $(-1, -1, -1)$

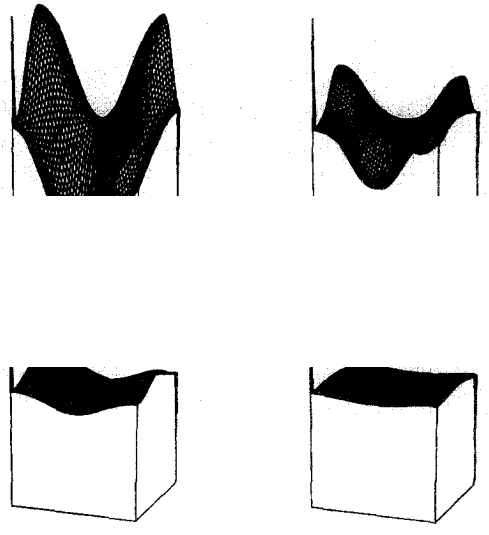

FIG. 10. Collapse of surface under mean curvature: $F(K) = -K$, surface at $T = 0.0, 0.3, 0.6, 0.9$.

and upper back right corner (1., 1., 1). We evolve the surface according to Eqs. (3.1) (3.3), with $F(K) = 1$, $\Delta t = 0.01$, and $N_{\text{point}} = 30$ points per side of the domain. The solution to this problem is just a sphere whose radius r is increasing at the constant rate $dr/dt = 1$. In Fig. 11 (Figs. 11a and 11b), we show the front at various times. (In the display of all of the following three-dimensional plots, the axes shown are for orientation purposes only and are not necessarily located at the real origin of the figure). As expected, the sphere expands smoothly. Of particular interest are the three surfaces in Fig. 11b. As the sphere expands, part of its boundary intersects the edge of the computational domain. This is reflected in the slicing of the level surface $\psi = 1$ by the sides of the box. This demonstrates the advantage of an upwind formulation: since information flows into the boundary, the surface does not know about the boundary, and the interior points of the level surface proceed unharmed.

C. *Level Surface, Torus, $F(K) = 1 - \varepsilon K$*

We evolve the toroidal initial surface, described by the set of all points (x, y, z) satisfying

$$z^2 = (R_0)^2 - ((x^2 + y^2)^{1/2} - R_1)^2,$$

where $R_0 = 0.5$ and $R_1 = 0.05$. Again we stress that we are following an entire family of concentric tori. This is a torus with main radius 0.5 and smaller radius 0.05. Again, to save labor, the initialization may be analytically expressed. The computational domain is a rectangular parallelpiped with lower left corner $(-1, -1, -0.8)$ and upper right corner (1., 1., 0.8). We evolve the surface with $F(K) = 1 - \varepsilon K$, $\varepsilon = 0.01$, $\Delta t = 0.01$, and $N_{\text{point}} = 90$ points per x and y side of the domain and the correct number in the z direction so that the mesh is uniform. Physically, we might think of this problem as the boundary of a torus separating products on the inside from reactants outside. Here, K is the mean curvature. In Fig. 12 (Figs. 12a and 12b), we plot the surface at various times. First, the torus burns smoothly (and reversibly) until the main radius collapses to zero. At that time ($T = 0.3$), the genus goes from 1 to 0, characteristics collide, and the entropy condition is automatically invoked. The surface then looks like a sphere with deep inward spikes at the top and bottom. These spikes open up as the surface moves, and the surface approaches the asymptotic spheroidal shape. Again, when the expanding torus hits the boundaries of the computational domain, the level surface $\psi = 1$ is clipped by the edges of the box. In the final frame ($T = 0.8$), the edge of the box slices off the top of the front, revealing the smoothed inward spike.

D. *Level Surface, Sphere and Torus, $F(K) = -K$, Mean Curvature*

Finally, we show the flow of two surfaces under their mean curvature. This problem has been studied extensively, see [2, 11]. First, we evolve the initial sphere of radius 1.0 moving with speed $F(K) = -K$. We use $N_{\text{point}} = 50$ uniformly in each

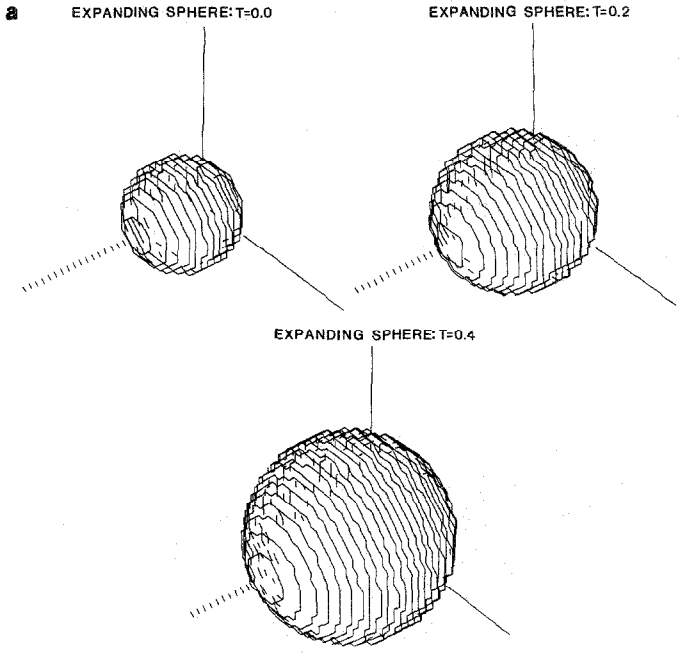

FIG. 11a. Sphere burning outwards (Beginning): $F(K) = 1$, surface at $T = 0.0, 0.2, 0.4$.

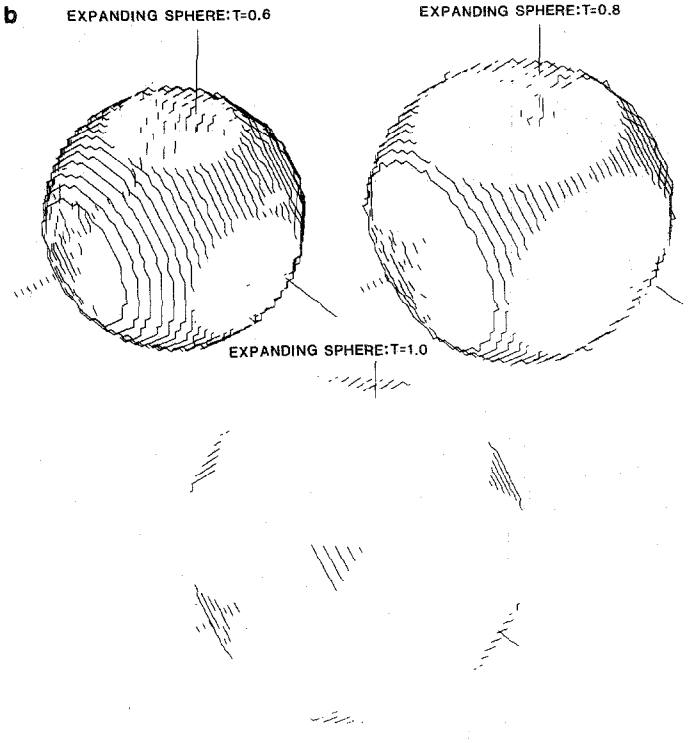

FIG 11b. Sphere burning outwards (Continued): $F(K) = 1$, surface at $T = 0.6, 0.8, 1.0$.

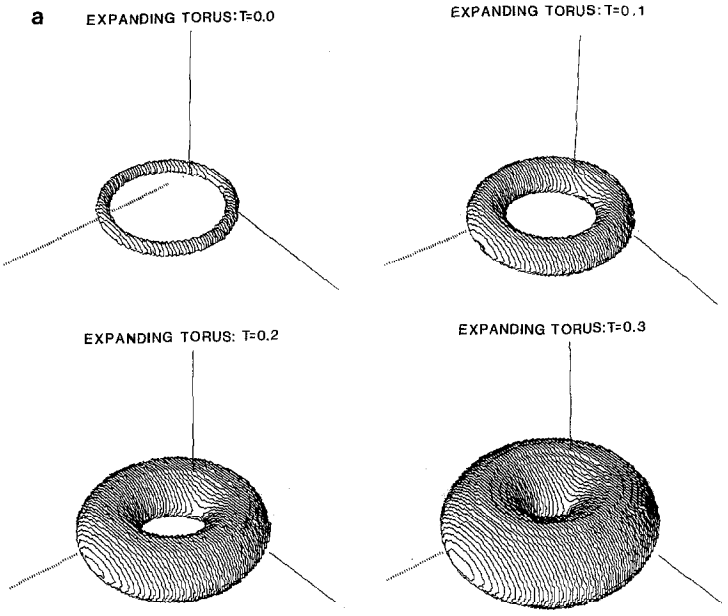

FIG. 12a. Burning Torus: Change of Topology (Beginning): $F(K) = 1 - \varepsilon K$, $\varepsilon = 0.01$, surface at $T = 0.0, 0.1, 0.2, 0.3$.

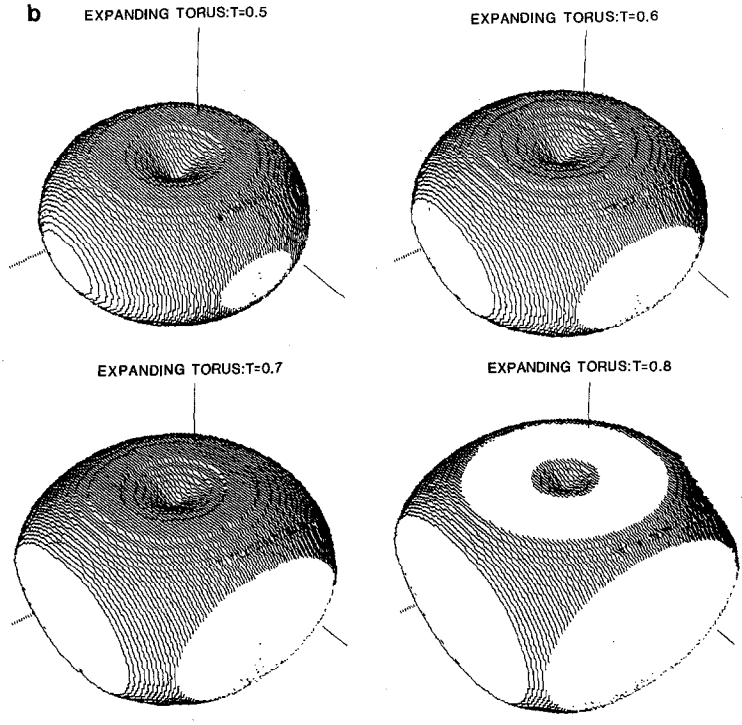

FIG. 12b. Burning torus: change of topology (Continued): $F(K) = 1 - \varepsilon K$, $\varepsilon = 0.01$, surface at $T = 0.5, 0.6, 0.7, 0.8$.

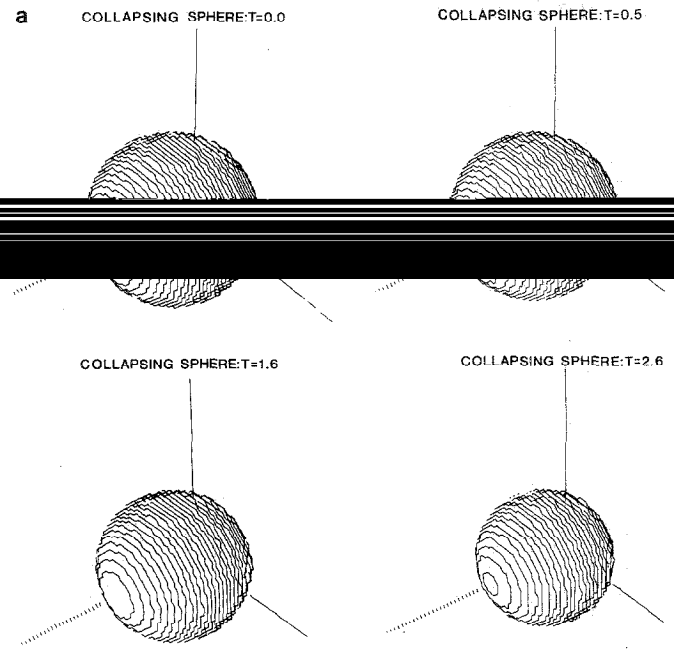

FIG. 13a. Sphere collapsing under mean curvature (Beginning): $F(K) = -K$, surface at $T = 0.0$, 0.5, 1.6, 2.6.

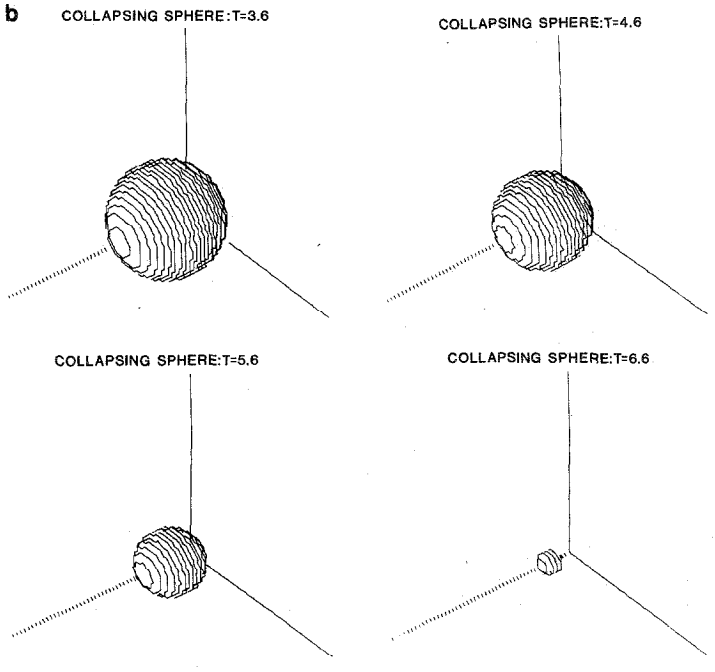

FIG. 13b. Sphere collapsing under mean curvature (Continued): $F(K) = -K$, surface at $T = 3.6$, 4.6, 5.6, 6.6.

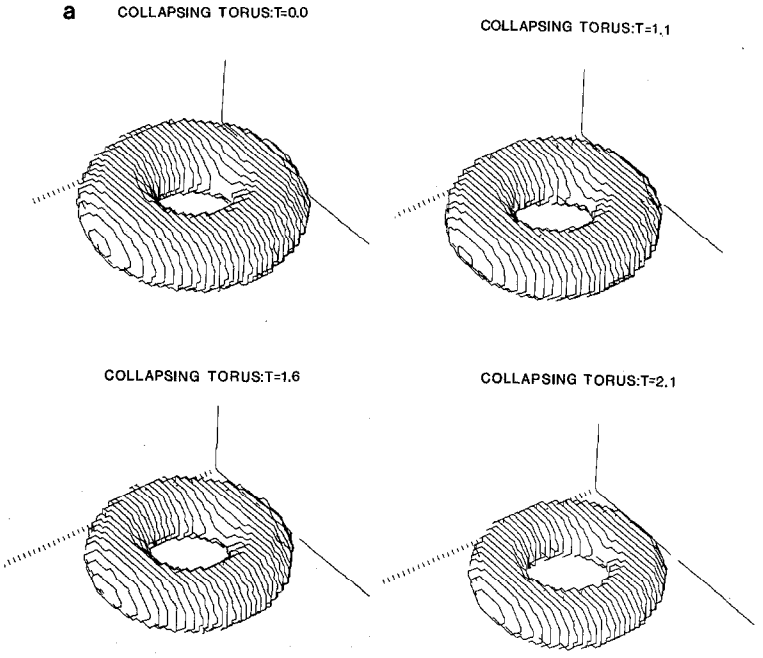

FIG. 14a. Collapse of torus under mean curvature (Beginning): $F(K) = -K$, $T = 0.0, 1.1, 1.6, 2.1$

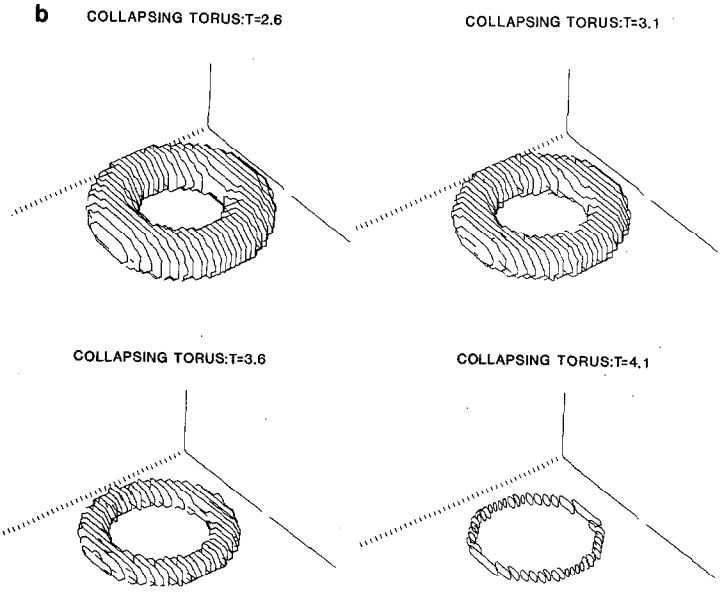

FIG. 14b. Collapse of torus under mean curvature (Continued): $F(K) = -K$, $T = 2.6, 3.1, 3.6, 4.1$

coordinate direction, and time step $\Delta t = 0.01$. Again, time is scaled by a factor of 100 because the real solution goes so fast. By symmetry arguments, the evolving surface should be a sphere of decreasing radius which eventually disappears. In Fig. 13 (Figs. 13a and b), we show the collapsing sphere at various times. As easily seen, the radius decreases slowly at first and very quickly at the very end. The final shape shown ($T = 6.6$) is the smallest surface that can be resolved on the given mesh size.

Finally, we evolve a toroidal initial surface under its mean curvature. The inner radius is 0.25 and the outer radius is 0.5. We embed the problem in a unit cube of side length 2. and use a fairly coarse mesh of $N_{\text{point}} = 45$ per side and time step $\Delta t = 0.01$. In Fig. 14 (Figs. 14a and b), we show the surface of the front at various times. For our particular initial surface, the torus deflates smoothly and collapses to the ring shown at $T = 4.1$ before it vanishes.

Summary

We have presented a class of algorithms, called PSC schemes, for moving surfaces under their curvature. These algorithms rely on numerically solving Hamilton–Jacobi equations with viscous terms, using approximation techniques from hyperbolic conservation laws. To demonstrate our techniques, we compute the solution to a variety of surface motion problems. We hope that this tool can be applied in several areas, such as flame stretch, vortex sheet rollup, Hele–Shaw cells, and crystal growth.

Copies of the computer program are available from the second author. All calculations were performed at the University of California, Berkeley and at the Lawrence Berkeley Laboratory.

APPENDIX: Instability of Marker Particles

Here, we analyze in some detail the difficulties inherent in a marker particle discretization of any Hamilton–Jacobi equation, and relate this to the motion of a front moving with constant speed. Consider the general Hamilton–Jacobi equation

$$\psi_t + H(\psi_x) = 0 \tag{A.1}$$

with smooth initial data $\psi(x_0(s), 0) + \psi_0(s)$. The method of characteristics tells us that ψ_x is constant along curves in x, ψ space defined by

$$\begin{aligned} \frac{\partial x}{\partial t} &= H'(\psi_x), \qquad x(s, 0) = x_0(s) \\ \frac{\partial \psi}{\partial t} &= \psi_x H'(\psi_x) - H(\psi_x) \end{aligned} \tag{A.2}$$

Following our notation in Section II, we define $g = (x_s^2 + y_s^2)^{1/2}$ and $\theta = \tan^{-1}(y_s/x_s)$, where now $x = x(s, t)$ and $\psi = \psi(s, t)$. This leads to a generalization of Eqs. (2.3)–(2.4) with $F(K) = 1$, namely

$$\begin{aligned} \theta_t &= 0 \\ g_t &= -[(\cos\theta)^{-3} H''(\tan\theta)]/\theta_s. \end{aligned} \tag{A.3}$$

For a curve moving with constant speed, $H''(\tan(\theta)) = -(\cos\theta)^{-3}$, and the system becomes linear, that is,

$$\begin{bmatrix} \theta \\ g \end{bmatrix}_t = \begin{bmatrix} 0 & 0 \\ 1 & 0 \end{bmatrix} \begin{bmatrix} \theta \\ g \end{bmatrix}_s. \tag{A.4}$$

This is a slightly ill-posed non-strictly hyperbolic system. However, the exact solution is easily seen to be

$$\theta = \theta_0(s), \qquad g = g_0(s) + t\theta_0'(s) \tag{A.5}$$

which "loses" a derivative.

This linear ill-posedness is manifested by $g(s, t)$ becoming zero, which corresponds to the intersection of characteristics in the original problem (Eq. (A.1)) at time $t = t_{\text{crit}} = \min(-g_0(s)/(\theta_0'(s))^-)$, as in Eq. (2.5).

For general concave ($H'' < 0$) Hamilton–Jacobi equation, this occurs at

$$t_{\text{crit}} = \frac{1}{\max[-H''((\psi_0)_x)(\psi_0)_{xx}]}$$

and is hence determined by the *second* derivative of the initial curve, when written as $y = \psi(x, 0)$. This is a subtle point, which we illustrate by example. Consider the flat initial data

$$y = 0 \equiv \psi_0(x).$$

The true solution to a unit speed moving front with this initial data is just $x \equiv s$, $y \equiv s + t$. We now consider a sequence of initial data which converge to the above flat data as the initial space step is refined. Take the initial data

$$y_0 = -\Delta s(\sin(\Delta s)^{1/2}) = y_0(\Delta s) = -y_0(2\,\Delta s) = -y_0(3\,\Delta s)$$

and $y_0(j\,\Delta s) \equiv y_0((j-4)\,\Delta s)$ for all j, and

$$x_0(j\,\Delta s) \equiv j\,\Delta s \cos((\Delta s)^{1/2})$$

defined on the grid $j\,\Delta s = 0, \pm 1, \pm 2, \ldots$. As $\Delta s \to 0$, the discrete initial data converges to the flat line $\psi = 0$ in the following fashion:

$$y_0(j\,\Delta s) = 0 + O((\Delta s)^{3/2})$$
$$y_0'(j\,\Delta s) = 0 + O((\Delta s)^{1/2})$$
$$x_0(j\,\Delta s) = x + O(\Delta s)$$
$$x_0'(j\,\Delta s) = 1 + O(\Delta s).$$

However, a marker particle numerical scheme (without regridding) blows up after $O(1/(\Delta s)^{1/2})$ time steps. With any relationship between Δt and Δs of the form $\Delta t = (\Delta s)^p$, $p > \frac{1}{2}$, the actual numerical blow up time is $O(\Delta t)O(1/(\Delta s)^{1/2}) = O(\Delta s)^{p-1/2}$, which goes to zero as Δs vanishes, even though the real solution is finite (in fact, zero in all derivatives) for all time.

APPENDIX B: General ENO Construction

We build R^M by induction on M. In each cell $x_j \leqslant x \leqslant x_{j+1}$, R^1 is defined as follows:

$$R^1(x; \Psi^n) = \Psi_j^n + (x - x_j)\, D_+ \Psi_j^n$$
$$= \Psi_j^n + (x - x_j)\, \Psi^n[x_j, x_{j+1}],$$

where $v[x_j - \mu, \ldots, s_j + v]$ denotes the usual coefficient in the Newton interpolating polynomial. We also define $k_{\min}^{(1)} = j$, $k_{\max}^{(1)} = j + 1$. Suppose we have defined $R^{M-1}(x; \Psi^n)$ for $x_j \leqslant x \leqslant x_{j+1}$, and also $k_{\min}^{(M-1)}$, $k_{\max}^{(M-1)}$ (the leftmost and rightmost indices, respectively). Then we compute

$$a^M = \Psi^n[x_{k_{\min}^{(M-1)}}, x_{k_{\max}^{(M-1)}+1}]$$
$$b^M = \Psi^n[x_{k_{\min}^{(M-1)}-1}, x_{k_{\max}^{(M-1)}}]$$

and proceed inductively.

If $|a^M| \geqslant |b^M|$, then in this interval

$$R^M(x; \Psi^n) = R^{M-1}(x; \Psi^n) + b^M \prod_{k=k_{\min}^{(M-1)}}^{k_{\max}^{(M-1)}} (x - x_k)$$

with $k_{\min}^M = k_{\min}^{(M-1)} - 1$, and $k_{\max}^M = k_{\max}^{(M-1)}$.

If $|a^M| < |b^M|$, then in this interval

$$R^M(x; \Psi^n) = R^{M-1}(x; \Psi^n) + a^M \prod_{k=k_{\min}^{(M-1)}}^{k_{\max}^{(M-1)}} (x - x_k)$$

with $k_{\min}^M = k_{\min}^{(M-1)}$, and $k_{\max}^M = k_{\max}^{(M-1)} + 1$.

To summarize, in each cell $x_j \leqslant x \leqslant x_{j+1}$, we have constructed an essentially non-oscillatory polynomial of degree M. This polynomial is the restriction to the cell of a polynomial interpolating (Ψ_v^n) at $M+1$ consecutive points x_v, including x_j and x_{j+1}; moreover, these points are chosen so that all derivatives of the polynomial are as small as possible in absolute value.

ACKNOWLEDGMENTS

We thank G. Barles, A. Chorin, O. Hald, M. Grayson, and P. L. Lions. In addition, we thank Bill Johnston and the Graphics Group at the Lawrence Berkeley Laboratory, University of California, Berkeley for help with the figures.

REFERENCES

1. G. BARLES, Report No. 464, Institut National de Recherche en Informatique et en Automatique (INRIA), Sophia Antipolis, France, 1985 (unpublished).
2. K. A. BRAKKE, *The Motion of a Surface by Its Mean Curvature* (Princeton Univ. Press, Princeton, NJ, 1978).
3 A. J. CHORIN, *J. Comput. Phys.* **57**, 472 (1985).
4. A. J. CHORIN, *J. Comput. Phys.* **35**, 1 (1980).
5. M. G. CRANDALL AND P. L. LIONS, *Math. Comp.* **43**, 1 (1984).
6. M. L. FRANKEL AND G. I. SIVASHINSKY, *Comb. Sci. Technol.* **29**, 207 (1982).
7. M. GAGE, *Duke Math. J.* **50**, 1225 (1983).
8. M. GAGE, *Invent. Math.* **76**, 357 (1984).
9. M. GAGE AND R. S. HAMILTON, *J. Differential Geom.* **23**, 69 (1986).
10. M. GRAYSON, *J. Differential Geom.* **26**, 285 (1988).
11. M. GRAYSON, A Short Note on the Evolution of a Surfaces via Mean Curvature, Stanford University Mathematics Dept. preprint (1987).
12. S. K. GODUNOV, *Mat. Sb.* **47**, 271 (1959).
13. A. HARTEN, B. ENGQUIST, S. OSHER, AND S. CHAKRAVARTHY, *J. Comput. Phys.* **71**, 231 (1987).
14. A. HARTEN, S. OSHER, B. ENGQUIST, AND S. CHAKRAVARTHY, *Appl. Num. Math.* **2**, 237 (1986).
15. G. HUISKEN, *J. Differential Geom.* **20**, 237 (1984).
16. N. N. KUTNETSOV, in *Topics in Numerical Analysis III*, edited by J. J. H. Miller (Academic Press, New York, 1977).
17. S. N. KRUZ'KOV, *Math. U.S.S.R. Sb.* **10**, 217 (1970).
18. L. LANDAU, *Acta Physiocochim. URSS* **19**, (1944).
19. J. S. LANGER, *Rev. Mod. Phys.* **52**, 1 (1980).
20. J. S. LANGER AND H. MULLER-KRUMHAAR, *Phys. Rev. A* **27**, 499 (1983).
21. P. D. LAX, *Comm. Pure Appl. Math.* **10**, 537 (1957).
22. G. H. MARKSTEIN, *J. Aero. Sci.* **18**, 199 (1951).
23. G. H. MARKSTEIN, *Non-Steady Flame Propagation* (Pergammon, MacMillan C., New York, 1964).
24. W. W. MULLINS AND R. F. SEKERKA, *J. Appl. Phys.* **34**, 2885 (1963).
25. F. A. NICHOLS AND W. W. MULLINS, *Trans. Metall. Soc. AIME* **223**, 1840 (1965).
26. W. NOH AND P. WOODWARD, in *Proceedings, Fifth International Conference on Fluid Dynamics*, edited by A. I. van de Vooran and P. J. Zandberger (Springer-Verlag, New York/Berlin, 1976).
27. S. OSHER, *SIAM J. Num. Anal.* **21**, 217 (1984).
28. O. A. OLEINIK, *T. Moscow Mat. Obsc.* **5**, 433 (1956).
29. C. SHU AND S. OSHER, *J. Comput. Phys.* **77**, 439 (1988).

30. B. R. PAMPLIN, *Crystal Growth.* (Pergammon, New York, 1975).
31. J. A. SETHIAN, Ph.D. dissertation, University of California, Berkeley, California; CPAM Rep. 79, June 1982.
32. J. A. SETHIAN, *Commun. Math. Phys.* **101**, 487 (1985).
33. J. A. SETHIAN, in *Variational Methods for Free Surface Interfaces*, edited by P. Concus and R. Finn (Springer-Verlag, New York, 1987).
34. J. A. SETHIAN, *J. Comput. Phys.* **54**, 425 (1984).
35. J. A. SETHIAN, in *Computational Fluid Mechanics and Reacting Gas Flows*, edited by B. Engquist, A. Majda, and S. Osher (Institute for Mathematics and Its Applications, Univ. of Minnesota, (1986).
36. J. A. SETHIAN AND S. OSHER, Level Set Algorithms for Hele-Shaw Flow, *J. Comput. Phys.*, in preparation.
37. G. I. SIVASHINSKY, *Acta Astronaut.* **4**, 1177 (1977).
38. D. TURNBULL, in *Solid State Physics* **3**, edited by F. Seitz and D. Turnbull, (Academic Press, New York, 1956).
39. N. J. ZABUSKY AND E. A. OVERMAN, *J. Comput. Phys.* **52**, 351 (1984).
40. Y. B. ZELDOVICH, *Comb. Flame* **40**, 225 (1981).